Journal of Hydrology 608 (2022) 127569

Contents lists available at ScienceDirect

Journal of Hydrology

journal homepage: www.elsevier.com/locate/jhydrol

Research papers

Evaluation of Sentinel-1, SMAP and SMOS surface soil moisture products for distributed eco-hydrological modelling in Mediterranean forest basins

José Gomis-Cebolla [a,*], Alicia Garcia-Arias [a], Martí Perpinyà-Vallès [b], Félix Francés [a]

[a] Research Institute of Water and Environmental Engineering (IIAMA) , Universitat Politècnica de València, Camí de Vera s/n, 46022 València, Spain
[b] Lobelia Earth, Parc Tecnològic Barcelona Activa, Carrer de Marie Curie 8, 08042 Barcelona, Spain

ARTICLE INFO

Keywords:
Surface soil moisture
Remote sensing
Spatial patterns
Eco-hydrological modelling
Multi-variable calibration

ABSTRACT

Reliable distributed hydrological modeling, especially in semi-arid areas, must consider the inclusion of surface soil moisture (SSM) spatial information during the calibration process. This variable plays a key role in the evapotranspiration processes that determine the hydrological cycle. The coarse resolution of the SSM estimates by satellite remote sensing has restricted the application of this approach to only large basins, focusing most of the studies in the consideration of simply the temporal dynamics of this variable. The growing efforts in providing higher spatial resolution through disaggregating methodologies or new sensor estimates facilitates the application of this spatial approach to small basins. This paper explores the applicability of the currently available satellite surface soil moisture estimates for distributed eco-hydrological modelling in Mediterranean forest basins. On one hand, this study contributes to fill the existing research gap on the use of remote sensing SSM spatial patterns within the distributed hydrological modelling framework in small basins. On the other hand, it serves as an indirect validation method for the spatial performance of satellite SSM products. To achieve this goal, we implemented the eco-hydrological model TETIS in three case studies named: Hozgarganta (southern Spain), Ceira (western Portugal) and Carraixet (eastern Spain). The SSM estimates selected for comparison were Sentinel-1 SSM provided by the Copernicus Global Land Services (CGLS), SMAP SSM disaggregated using Sentinel-1 (SPL2SMAP_S) provided by the National Aeronautics and Space Administration (NASA), SMOS SSM provided by the Barcelona Expert Center (BEC), and SMOS and SMAP SSM disaggregated using the DISPATCH algorithm provided by Lobelia Earth. The methodology employed involved a multi-objective and multi-variable calibration in terms of remote sensing SSM spatial patterns and in-situ streamflow, using the Spatial Efficiency Metric (SPAEF) and the Nash-Sutcliffe efficiency index (NSE) respectively. Before model calibration a sensitivity analysis of the most influent variables was performed. The temporal and spatial comparison of the reference SSM products revealed inconsistencies amongst products. The disaggregating methodology determined the spatial agreement to a greater degree than the sensor itself (i.e. SMAP, SMOS). In spite of the differences amongst products, the multi-objective calibration approach proposed increased the robustness of the hydrological modelling.

1. Introduction

The reliable determination of the hydrological variables in a catchment has been a challenging objective for a long time. Many hydrological models have emerged as a response to growing demand of operational tools. Amongst them, deterministic distributed hydrological models offering spatial explicit predictions can fulfil the lack of spatial representation of the dominant hydrological processes when available in-situ observations are not sufficient. Traditionally, hydrological model calibration was based on solely streamflow information. However, this does not guarantee the correct representation of the spatial heterogeneity of other state variables (Rajib et al., 2016; Wambura et al., 2018). The introduction in hydrological models of satellite derived information has the potential to overcome this limitation by improving models performance, both temporally and spatially (Laiolo et al., 2016; Lopez et al., 2017; Herman et al., 2018; Dembelé et al., 2020a). Additionally, it should not be ignored the existing relationship between vegetation dynamics and the related hydrological processes. Thus, vegetation requires proper representation in eco-hydrological models to attend reliability requirements in catchments with representative areas of forestry or

* Corresponding author.
E-mail address: jgomceb@iiama.upv.es (J. Gomis-Cebolla).

https://doi.org/10.1016/j.jhydrol.2022.127569
Received 1 October 2021; Received in revised form 28 January 2022; Accepted 31 January 2022
Available online 5 February 2022

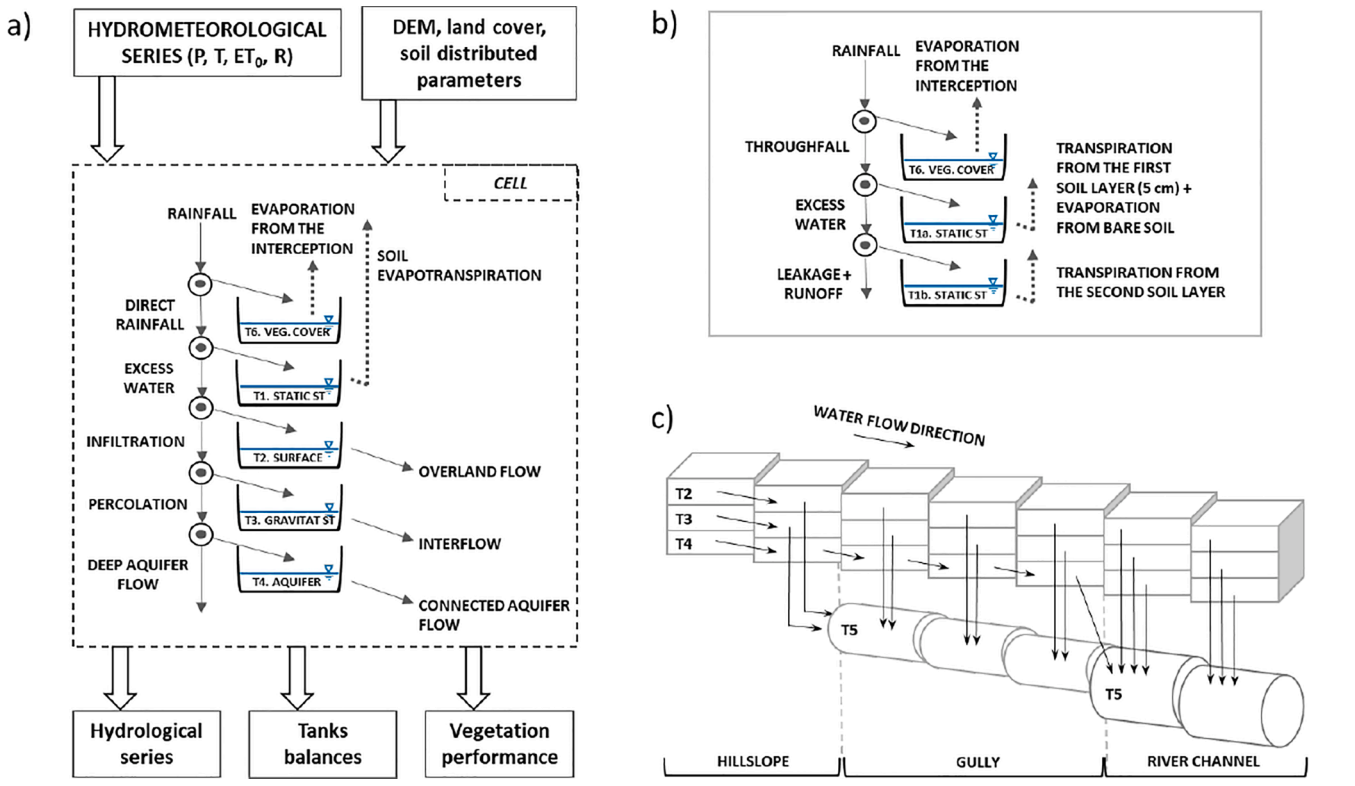

Fig. 1. Conceptual scheme of the TETIS hydrological model (a), diagram of the hydrological sub-model for ECO-TETIS (b) and bidimensional simplification of the horizontal flow for TETIS (c).

agricultural uses (Pasquato et al., 2015; Ruiz-Pérez et al., 2017; Bai et al., 2018).

The surface soil moisture information derived from satellite data has been commonly employed for improvement in the hydrological modelling, due to its importance in the description of the hydrological cycle (GCOS, 2019), especially in semi-arid areas. This has been mostly done via assimilation (Laiolo et al., 2016; Alvarez-Garreton et al., 2016; Abbaszadeh et al., 2020; Khaki et al., 2020) or direct calibration approaches (Wanders et al., 2014; Silvestro et al., 2015; Rajib et al., 2016; Lopez et al., 2017; Dembelé et al., 2020a). Most of the studies have focused on the temporal dynamics of the SSM, mainly due to the coarse spatial resolution of the available estimates. Special attention to spatial patterns was restricted only to large basins (Dembelé et al., 2020a). The growing efforts in providing higher spatial resolution through disaggregating methodologies (Merlin et al., 2013;; Piles et al., 2011;Piles et al., 2012; Das et al., 2019) or new sensor estimates (Bauer-Marschallinger et al., 2019) allow to provide operational estimations at 1 km, which is an accepted basic assumption for eco-hydrological resources management (Sabaghy et al., 2020). Thus, the emerging research performed in hydrological model evaluation and calibration based on spatial patterns (Koch et al.,2015; Mendiguren et al., 2017; Demirel et al., 2018; Koch et al., 2018; Zink et al., 2018), can be transferred to SSM for medium and small basins. However, there is an underlying uncertainty in current SSM products (Fang et al., 2016; Al-Yaari et al., 2019; Wang et al., 2021) and model performance is dependent on the selection of the reference product used for calibration (Dembelé et al., 2020b). In consequence, a previous analysis of their performance before the calibration process is necessary.

This paper is aimed at the evaluation of the current available satellite soil moisture products (at 1 km spatial resolution) for distributed eco-hydrological modelling in Mediterranean basins. Firstly, it contributes to fill the existing research gap on the use of remote sensing SSM spatial patterns within the distributed hydrological modelling framework in small basins. Secondly, it serves as an indirect validation method of the spatial performance of satellite SSM products. To achieve these goals, we selected TETIS hydrological model (Francés et al., 2007), which is a conceptual deterministic model. In its tanks structure, processes are represented by parameters that are physically based and spatially distributed. It has a dynamic vegetation sub-model (Pasquato, 2013; Pasquato et al., 2015) and has been implemented in several case studies (e.g. Ruiz-Pérez et al 2016; Ruiz-Pérez et al., 2017; Puertes et al., 2019; Echeverría et al., 2019; Barrientos et al 2020). Echevarria et al (2019) stated the possibility of calibrating the TETIS model basing exclusively in satellite information. Three case studies, named Carraixet (eastern Spain), Hozgarganta (southern Spain), and Ceira (western Portugal), have been strategically selected to perform this research in the Mediterranean Region. Four different sources of SSM estimates were considered for the study: Sentinel-1 SSM provided by Copernicus Global Land Services (CGLS), SMOS SSM provided by the Barcelona Expert Center (BEC), SMAP SSM disaggregated using Sentinel-1 provided by NASA, and SMOS and SMAP SSM disaggregated using the DISPATCH algorithm provided by Lobelia Earth. The methodology employed involved a multi-objective, multi-variable calibration in terms of remote sensing SSM spatial patterns and in-situ streamflow.

The paper contents are organised as follows: section 2 introduces TETIS eco-hydrological model. Section 3 deals with the description of the study sites and the data employed in TETIS implementation together with a description of the SSM products considered. It includes the methodology employed for the remote-sensing SSM product comparison, model calibration steps (sensitivity analysis, calibration experiments and assessment metrics) and model evaluation. Section 5 and 6 provide the results and their discussion respectively. Finally, section 8 summarizes the main conclusions derived from this study.

2. TETIS eco-hydrological model

TETIS is a hydrological conceptual distributed model useful for both for flood event and continuous simulation. The TETIS model bases the

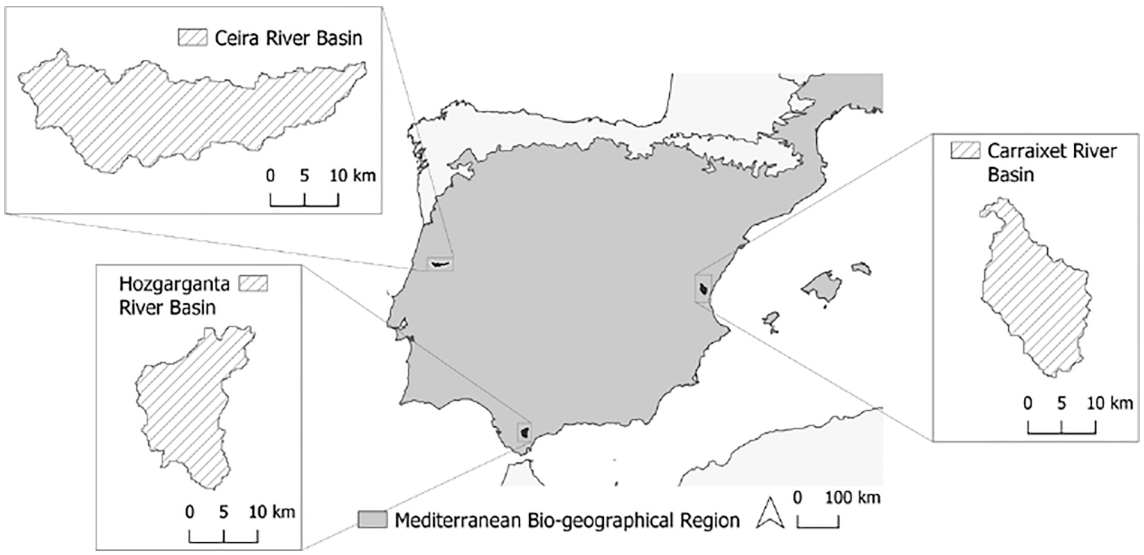

Fig. 2. Study sites location in the Mediterranean Bio-geographical region of the Iberian Peninsula: Ceira River basin (northwestern Portugal), Hozgarganta River basin (southern Spain), and Carraixet River basin (eastern Spain).

runoff production on the water balance calculation for each cell. The water is assumed to be distributed in six conceptual storage tanks interconnected (Fig. 1a). The tanks represent the capacity in the water storage by the vegetation cover (T6), the static storage (T1), the surface storage (T2), the gravitational storage (T3) and the aquifer (T4). The sixth tank (T5) represents the channel when it exists in the cell as shown in Fig. 1c.

The water volumes (H) stored in each tank are the state variables of the model. TETIS has a modular structure. In consequence, these H states depend on the conceptual schema adopted. Due to the spatially distributed conceptualization, the morphological and hydrologic characteristics of the soil in each cell also determine H states.

The modules in TETIS are conceptualized as an interconnected three-dimensional mesh. T2, T3 and T4 drain into the corresponding downstream one, following the flow directions proposed by the digital elevation model (DEM) and reaching the drainage network that consists of gullies and channels (Fig. 1c). The cases where the destination cell is a gully, both the overland flow and interflow integrate into it while the base flow drains to the downstream cell. In channel cells all the output flows integrate into the river channel tank (T5). Threshold areas are parametrized to discriminate between these three types of cells: hillside, gullies, and river channel. Summarizing, runoff translation along the basin considers that non-abstracted water circulates on the hillslopes until to the natural drainage network of the basin is reached. Onwards, water flows through the drainage network itself. Conceptual simplifications of the laws of the Hydraulics in natural channels are included in TETIS. The kinematic wave supports the TETIS modelling approach assuming uniform flow, and comparable friction and channel slopes. As a simplification of the Saint-Venant shallow-water equations, the kinematic wave integrated in TETIS neglects the terms corresponding to inertial and pressure effects in the equation of conservation of energy. On the other hand, the hydraulic characteristics of the riverbeds are parametrized in TETIS. Consequently, characteristic geomorphological information of the basins can be accounted for.

The eco-hydrological configuration of TETIS includes a dynamic vegetation model in which the static storage tank (T1) splits into two tanks (Fig. 1b) associated to the different layers found in the first horizons of the soil: the shallow static storage (T1a), the deep static storage (T1b). T1a involves the processes of evaporation from the bare soil and superficial roots transpiration from the first few centimeters of the soil. T1b considers the deep roots transpiration processes from the underlying layer.

In T6 the balance of the water stored by the canopy is balanced in terms of rainfall and evaporation from the interception considering the LAI. The LAI is also dynamically estimated by the dynamic vegetation model. TETIS plant biomass production (Pasquato et al., 2015) is based on the use of the light use efficiency (LUE) concept and defined in Equation (1).

$$\frac{dB_l}{dt} = (LUE \cdot \varepsilon \cdot PAR \cdot fPAR - Re) \cdot \varphi_l(B_l) - k_l B_l \quad (1)$$

where B_l (gDM.m^{-2}) represents the leaf biomass and LUE is given in gDM.MJ^{-1}.d^{-1}. PAR is the photosynthetic active radiation (MJ.m^{-2}), fPAR is the fraction of PAR absorbed by the vegetation calculated from the Beer-Lambert law. ε is a stress factor that mainly includes moisture (and temperature) stress effects linking the hydrological changes to the vegetation performance in water-controlled systems. Re is the respiration (gDM.m^{-2}) based on tissue specific C:N ratios, air temperature and phenology according to Sitch et al. (2003). $\varphi_l(B_l)$ represents the fractional leaf allocation and is calculated by the model as $1 - Lai_{max}/Lai$. k_l (d^{-1}) is the leaf natural decay factor used to consider the senescence. Scaling B_l by the specific leaf area, SLA (m^2.gDM^{-1}), and by the vegetation fraction cover, fc between 0 and 1, LAI is finally obtained (eq. (2)).

$$LAI = B_l \cdot SLA \cdot f_c \quad (2)$$

3. Study sites description and data

3.1. Study sites

Three study sites (Fig. 2) were selected to be representative of the climatology and the hydrology of the Mediterranean Bio-geographical region in the Iberian Peninsula: Ceira River basin (northwestern Portugal), Hozgarganta River basin (southern Spain), and Carraixet River basin (eastern Spain). The extension covered by natural land uses (i.e. with no human influence) represents at least 50% (Fig. 3). This fact enables to perform the comprehensive analysis proposed in this paper as precisely in these pixels there is a concordance on what TETIS is simulating and the remote sensing SSM observations (i.e. SSM driven by precipitation with no influence of irrigation). Apart from this, the spatial distribution of the stations (Fig. 3) properly represents the meteorological dynamics (Table 1) in each basin. Data is provided quality controlled by the responsible institutions (Table 2).

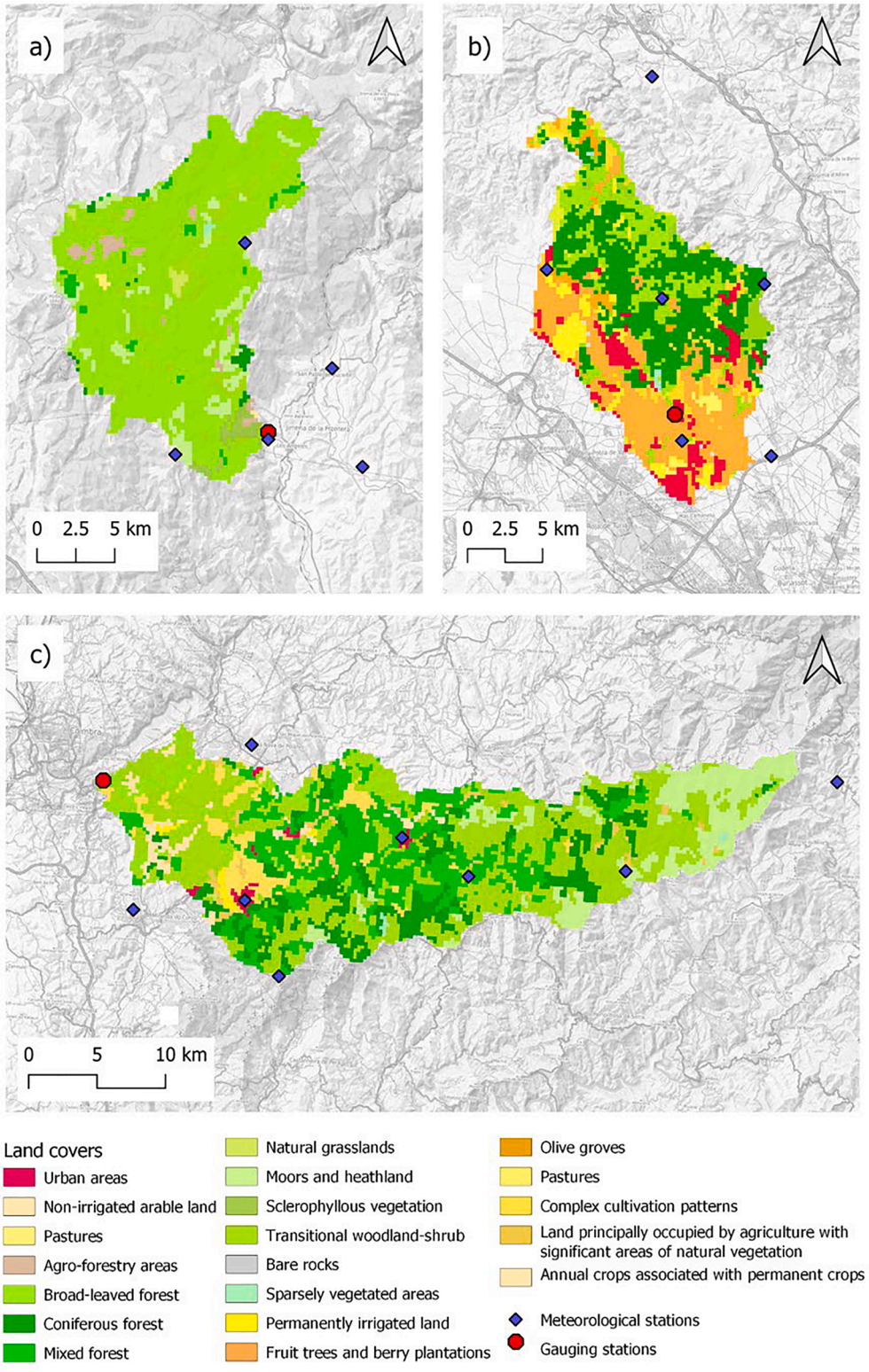

Fig. 3. Land cover, meteorological stations and gauging stations in the case studies: a) Hozgarganta River basin (Spain), b) Carraixet River basin (Spain), and c) Ceira River basin (Portugal).

The Hozgarganta River starts at the confluence of the La Sauceda gorge (Province of Málaga, Spain) and the Pasada Llana canyon at 160 m.a.s.l. This river collects water from the Los Alcornocales Natural Park in the province of Cádiz (Spain). After 45.6 km in natural regime, it discharges to the Guadiaro River, which drains to the western Mediterranean Sea. The Hozgarganta river basin extends over approximately 228.3 km^2 of forestry main land uses dominated by coniferous, broad-leaved, and mixed forests, with some isolated presence of natural grasslands, moors and heathland, sclerophyllous vegetation, transitional woodland-shrub, pastures, and agro-forestry areas. The gauging station with the same name, Hozgarganta (280189, 4034238 in ETRS89/UTM zone 30 N, EPSG 25830) allows the consideration of the complete

Table 1
Meteorological characterization of the case studies considering years between 2016 and 2020.

Case study	Annual mean temperature (°C)	Annual precipitation (mm)	Annual reference evapotranspiration (mm)
Hozgarganta River basin	17.7 ± 0.4	826 ± 278	1212 ± 41
Ceira River basin	14.0 ± 0.3	706 ± 328	412 ± 3
Carraixet River basin	16.6 ± 0.1	373 ± 108	1142 ± 11

Table 2
Model input data used in study cases distributed parameter estimation. Original spatial resolution of source files is indicated in parenthesis. Dd refers to drainage directions, cda to accumulated drainage cells, so to slope, u to hillslope velocity ($m.s^{-1}$), wp to wilting point (mm), fc to field capacity (mm), opt to optimum point (mm), Ks to infiltration capacity ($mm.h^{-1}$), Kss ($mm.h^{-1}$) to interflow velocity, Kp to percolation capacity ($mm.h^{-1}$), Ksa to saturated hydraulic conductivity ($mm.h^{-1}$) and Kps to deep aquifer flow ($mm.h^{-1}$), swd to surface water detention (mm), fvc to vegetation fraction cover, P to precipitation (mm), T to air temperature (°C), ETO to reference evapotranspiration (mm), SR to solar radiation ($MJ.m^{-2}.d^{-1}$) and Q to discharge ($m^3.s^{-1}$).

	Source	TETIS distributed parameter
DEM	EU-DEM v.1 (25 m)	dd, cda, so, u
Land Cover	Corine Land Cover 2018 (100 m)	Land use, fc,wp, opt
Soil properties	3D-Eurosoils (250 m)	Ks, Kss, fc, wp, opt
	GLHYMPS.V2.0 (geodatabase)	Kp, Ksa, Kps
	Soilsgrids (250 m)	swd, porosity
Vegetation	Landsat GEE (30 m)	fvc
Hydro-meteo	SiAR, SAIH-HIDROSUR, SAIH Júcar, SNIRH	P , T , ET_0, SR, Q

natural drainage area of this tributary. Elevation range between 38 and 1042 m above the sea level (m.a.s.l) (EU-DEM v1.1). The annual rainfall of data analysed in this research ranges between 550 and 1100 mm, and the reference evapotranspiration is close to 1200 mm. As is frequent in Mediterranean basins, rainfall between October and April is intense while summer is a dry season. In consequence, Hozgarganta suffers relevant runoff reduction in the upper basin during summer. In contrast, many pools and ponds remain permanent sustaining the local fauna. Mesozoic and Cenozoic eras represent the lithology that frame the hydrogeology in the Aljibe unit, where the presence of characteristic sandstones and clays determine the low permeability of the basin.

The Ceira River basin is a tributary of the Mondego River and their confluence is situated slightly upstream the city of Coimbra (Portugal). Ceira River springs in the Açor Mountains System, near Pióddão village (1300 m.a.s.l.). During its 106 km haul, the mainstream of the Ceira River collects water from a catchment area of 496.89 km^2. Forestry main land uses dominate the basin, showing three main areas: the upper basin where transitional woodland-shrub dominate in combination with moors and heathlands areas with presence of coniferous and mixed forests; the middle basin where these forests gain relevance; and the lower basin where transitional areas and complex cultivation patterns cover most of the land surface. Ponte Cabouco gauging station (553466, 4447702 in ETRS89/UTM zone 29 N, EPSG 25829) provided enough and good quality hydrological information that revealed permanent flow (mean value 5.83 m^3/s) and occasional winter floods of relevant intensity. Elevation in the basin ranges between 62 and 1380 m.a.s.l (EU-DEM v1.1). Annual rainfall ranges in this research between 380 and 1040 mm (very dry years compared to historical references of annual rainfalls between 1000 and 1400 mm), and reference evapotranspiration is about 400 mm. Permeabilities are low or very low in the Ceira River catchment, with relevant presence of metamorphics and sedimentary rocks. Limestone, quartzite and Paleozoic gabbro, Tertiary-age deposits and terraces and gravels can be found all over the Maciço Antigo in the area.

The Carraixet River has its source at Gàtova and collects water from the southern Calderona mountain range in the province of Valencia (Eastern Spain). After 45 km, it drains directly into the Mediterranean Sea north to the city of Valencia. The Carraixet upper river basin extends over approximately 236.5 km^2 of forestry main land uses dominated by coniferous forests and transitional woodland-shrub areas. Natural grasslands and sclerophyllous vegetation represent lower stratums in the study site. Urban and agricultural uses dominate the lower basin with high presence of fruit trees plantations and complex cultivation patterns. The gauging station of Bétera (716948, 4387531 in ETRS89/UTM zone 30 N, EPSG 25830) is the perfect reference outlet to consider the study site well represented by natural land covers. Frequently absent base flow characterizes the hydrology, as it is common in Mediterranean ephemeral streams. Elevation in the basin ranges between 55 and 898 m.a.s.l (EU-DEM v1.1). Annual rainfall ranges between 270 and 480 mm approximately, while reference evapotranspiration ranges between 1000 and 1200 mm. This fact indicates the study site is clearly semiarid. Following the typical Mediterranean patterns, rainfall prevail in autumn and spring, while reference evapotranspiration stands out in spring and summer (the driest season). Two main areas highlight regarding the lithology: oldest formations dated as Triassic in the upper basin, and newest formations from the Quaternary in the lower basin. Conglomerates, sandstones, limestones and multi-colored clays, combined with gravel soils, conglomerates, sands and silts determine the hydrogeology. Karst intensity is determinant for the percolation processes in the basin.

Not relevant erosive processes take place in most of the basins surfaces since they are mature basins with morphological stability, just in upper basin of Hozgarganta some erosion risk can be deducted from huge slopes in the tributary gorges.

3.2. Input datasets and model setup

Table 2 summarizes model input data used for TETIS distributed parameter estimation. All the inputs were conveniently reprojected and resampled to accommodate to the model spatial resolution (250 m) and temporal resolution (1d). Regarding elevation data, they were obtained from the EU-DEM V.1 product available at https://land.copernicus.eu/imagery-in-situ/eu-dem/eu-dem-v1.1. Correction of the dem, if necessary, consisted in filling sinks and carving the reference river network. Derived parameters maps involved the drainage directions (dd), accumulated draining cells (adc), slope (s) and hillslope velocity (u) calculated as $\sqrt{2s}$. Land use information was obtained from the Corine Land Cover product 2018 release available at https://land.copernicus.eu/pan-european/corine-land-cover/clc2018, although some modifications were considered based on the Copernicus Global Land Service (CGLS) Land Cover product. This is the case of Ceira, in which burnt area pixels were reclassified with the most common pixel value of the CGLS for the period 2015–2020. For the case of Carraixet, Corine land cover the natural land uses pixels were reclassified based on the CGLS product. Resulting maps, were additionally compared to high resolution google earth images to ensure accuracy. Soil properties (field capacity (fc), witling point (wp) and saturated hydraulic conductivity (Ks)) were obtained from the 3D-Eurosoils product (Tóth et al., 2017) available at https://esdac.jrc.ec.europa.eu/content/3d-soil-hydraulic-database-europe-1-km-and-250-m-resolution. The corresponding field capacities and wilting points of the different soils depths provided by this database were conveniently regrouped in order to accommodate to the surface (first 5 cm) and deep layer (5 cm up to root depth or bedrock) of the model. Root depth was fixed for the different land uses. Optimum point was considered as 2/3 of field capacity. Ks and Kss were calculated as $1/Ks = (1/L)\sum b_i/KS_i$ and $Kss = (1/L)\sum b_i\hat{A}\cdot KS_i$, respectively,

where L refers to the total soil depth up to the bedrock, b_i the difference between consecutive depths and Ks_i the values of the saturated hydraulic conductivity for the seven depths. Depth to bedrock was obtained from soilgrids (Hengl et al., 2017)). Percolation capacity (Kp) was directly obtained from the GLHYMPS V.2.0 (Huscroft et al., 2018) available at https://dataverse.scholarsportal.info/dataset.xhtml?persistentId=doi:10.5683/SP2/TTJNIU. For the case of the saturated horizontal hydraulic conductivity (Ksa) and deep aquifer flow velocity (Kps) the following assumptions were considered: Ksa = Kp and Kps = 0.1Kp. Surface water detention was calculated according to Manfreda et al., 2005, considering the soil texture, slope and land use. Fractional vegetation cover was obtained from LANDSAT NDVI data directly in the google earth engine platform. NDVI was scaled between the NDVI values of a bare soil pixel ($NDVI_s$) and full vegetation cover pixel ($NDVI_\infty$) over the study region. Corresponding value of 0.13 and 0.85 respectively were selected for the three study regions. The mean value for the temporal period considered 2016–2020 was considered as TETIS input. Finally, hydro-meterological data was provided by the SAIH-Hidrosur (http://www.redhidrosurmedioambiente.es) for the case of Hozgarganta river and SAIH-Júcar (http://saih.chj.es/chj/saih/) for the case of Carraixet river. Temperature (T) and solar radiation (SR) data were obtained from the national system of agricultural information (SIAR) for the Spanish cases. In the case of Ceira river, all the information was provided by the Sistema Nacional de Informaçao de Recursos Hídricos (SNIRH). The different stations available for each basin are displayed in Fig. 3. Regarding the geomorphological relationships used in TETIS they were obtained from previous studies (Bussi et al., 2014). For Carraixet, the effect of transmission losses present in ephemeral rivers was taken into account by introducing a loss point per km along the main river channel. Transmission losses values were calculated following Neitsch et al. (2011). Mean river width for each kilometer and a channel effective hydraulic conductivity of 3.75 $mm.h^{-1}$ were considered for calculation.

3.3. Satellite products

3.3.1. Sentinel-1 SM

Sentinel-1 (S1) soil moisture data is obtained by applying the Technological University of Vienna (TU-Wien) change detection method (Wagner, 1998) to C-band Sentinel-1 backscatter time series which are collected in Interferometric Wade Swath (IW) and VV-polarization mode (Bauer-Marschallinger et al., 2019). In a first step, backscatter values are terrain-geo-corrected and radiometrically calibrated, then they are normalized to a reference incidence angle considering the linear slope parameter. Finally, relative soil moisture values (expressed in %, from 0 to 100) are derived by scaling the normalized backscatter values between the historically driest (dry reference) and wettest (wet reference) observed values. Output spatial resolution is 1 km. Pre-processing of these data consisted in two phases: spatial resampling to adequate to the considered spatial projection and translation to absolute soil moisture values considering soil porosity. Porosity information was obtained from SOILGRIDS bulk density following Das (2013). Soil moisture values were previously screened for already masked invalid pixels. Finally, daily values were monthly aggregated. To maximize the amount of data considered for the analysis, a month was considered valid if it had at least 3 available days. For the simplicity of notation, we will refer to this product as S1.

3.3.2. SMAP/S1

SMAP/Sentinel-1 L2 Radiometer/Radar Soil Moisture (SPL2SMAP_S level-2) product results from the merging of Soil Moisture Active Passive (SMAP) radiometer data with Sentinel-1A/1B radar data through an active/passive downscaling algorithm. This downscaling is obtained by two different approaches: baseline and optional. The baseline approach is focused on the disaggregation of the L-band brightness temperature from the SMAP Level-2 Enhanced product (L2_SM_P_E) at about 33 km spatial resolution in EASE2 9 km grid, using the fine resolution (at 1 km) Sentinel radar backscatter, which are collected in IW Swath mode and VV and VH polarization mode. The soil moisture is then retrieved by applying the Single Channel Algorithm at vertical polarization (SCA-V) to the downscaled brightness temperature. In the optional approach, the soil moisture available in L2_SM_P_E is directly disaggregated at 1 km using the sentinel backscatter cross-sections (Das et al., 2017). For the rest of the paper, we will refer to SMAP-BS for the baseline approach and SMAP-DIS for the optional approach. In an analogous way to Sentinel-1 SSM pre-processing consisted in spatial resampling to the reference spatial projection. For this case, as screening for invalid pixels considering only data with good quality reduced considerably the amount of available data, we decided to simply filter soil moisture values by an upper threshold given by porosity (same as in Sentinel-1 SSM) so we could discard possible outliers. Finally, daily values were monthly

Table 3
Parameter and associated ranges considered for sensitivity analysis. For the case of Hozgarganta and Ceira [100–5000] range was used for FC6, while for Carraixet [0.1–100] was considered.

Parameter	Range	Reference
FC1 – Maximum Static storage factor (–)	[0.8–1.5]	This study
FC2 – Evapotranspiration vegetation factor (–)	[0.8–1.5]	This study
FC3 – Infiltration capacity factor (–)	[0.2–1.2]	This study
FC4 – Slope velocity factor (–)	[0.2–1.2]	This study
FC5 – Percolation capacity factor (–)	[0.2–1.2]	This study
FC6 – Interflow hydraulic capacity factor (–)	[0.1–100] [100–5000]	This study
FC7 – Deep aquifer percolation capacity factor (–)	[0.2–1.2]	This study
FC8 – Connected aquifer hydraulic conductivity factor (–)	[100–5000]	This study
FC9 – Kinematic Geomorphological Wave factor (–)	[0.05–1.0]	This study
β – exponent soil water limitation function (–)	[1–3]	Williams & Albertson 2005
ξ – exponent vegetation water stress function (–)	[1–3]	Williams & Albertson 2005
I_{max} – maximum leaf interception storage (mm)	[0.2–1.2]	This study
% root – Roots ratio in the surface layer (%/100)	[0.1–0.5]	This study
k – light extinction coefficient (–)	[0.3–0.7]	(Ross, 1975)
T_{opt} – Optimum temperature (°C)	[10–30]	This study
LUE – Light Use Efficiency (gDM/MJd)	[1.3–2.7]	Copernicus DMP ATBD
rr – respiration rate (gC/gNd)	[0.02–0.08]	This study
k_l – the leaf natural decay factor (d^{-1})	[0.003–0.008]	This study
SLA – specific leaf area (m^2/gDM)	[0.01–0.03]	Heinsch et al., 2003
LAI_{max} – maximum LAI (m^2/m^2)	[0.5–3]	This study

aggregated. It is worth remembering at this stage that for calibration purposes we are dealing with monthly spatial patterns, therefore possible uncertainties due to these considerations are minimized.

3.3.3. SMOS-BEC

SMOS soil moisture data is provided by the Barcelona Expert Center (BEC). We have used the Level-4 product which provides estimates of SMOS soil moisture at 1 km across Europe. SSM estimates are obtained by applying a semi-empirical downscaling algorithm that relates the SSM to the brightness temperature, NDVI and LST (Piles et al., 2011; Piles et al., 2012). Inputs to the product are: BEC SMOS Level-3 soil moisture, that is directly generated by the L2 SMOS from ESA Expert Support Laboratory (ESL) after discarding invalid pixels and binning the data to the 25 km EASEv2 grid. Daily SMOS L1 brightness temperature (provided by ESA L1C at 25 km) at both horizontal and vertical polarization at the Earth surface at three incidence angles (32.5°, 42.5° and 52.5°). Daily LST or skin temperature at 12 h at around 9 km provided by the ECMWF model. 16-day TERRA MODIS NDVI at 1 km. During the process, some considerations are addressed such as sea-land contamination and gap-filling of original L3 soil moisture. For more information, we refer to the products description file (Pablos et al., 2020). Preprocessing consisted in spatial resampling, and monthly aggregation. SSM estimates were also filtered by an upper threshold provided by porosity. Ascending orbits (06:00 am) were used in this study. For notation simplification, we will refer this product as SMOS-BEC.

3.3.4. SMAP and SMOS DISPATCH

Alternatively, SMAP and SMOS soil moisture estimates at 1 km were obtained considering the DISaggregation based on a Physical and Theoretical scale Change (DISPATCH) algorithm (Merlin et al., 2013)). Two different low resolution Surface Soil Moisture (SSM) products were used in this study: the SMOS mission Level 2 swath-based SSM and the SMAP mission Enhanced Level 3 Radiometer Global Daily 9 km EASE-Grid SSM. Both products were used as input to the downscaling algorithm. DISPATCH disaggregates low-resolution SSM to higher resolution SSM by using a soil evaporative efficiency (SEE) term at higher resolution to model the spatial variability within a low-resolution pixel. SEE, defined as the ratio of actual to potential evaporation, is derived using Land Surface Temperature (LST) and Normalized Difference Vegetation Index (NDVI) data. The distribution of the high-resolution SSM around the mean value of the low-resolution SSM products is possible through the spatial link between the optical-derived SEE and SSM(Merlin et al., 2012) . In this study, the MODIS version-6 LST products onboard Terra (MOD11A1) and Aqua (MYD11A1) and NDVI product onboard Terra (MOD13A) were used to derive the 1 km SEE fields. DISPATCH also uses elevation data extracted from the GTOPO30

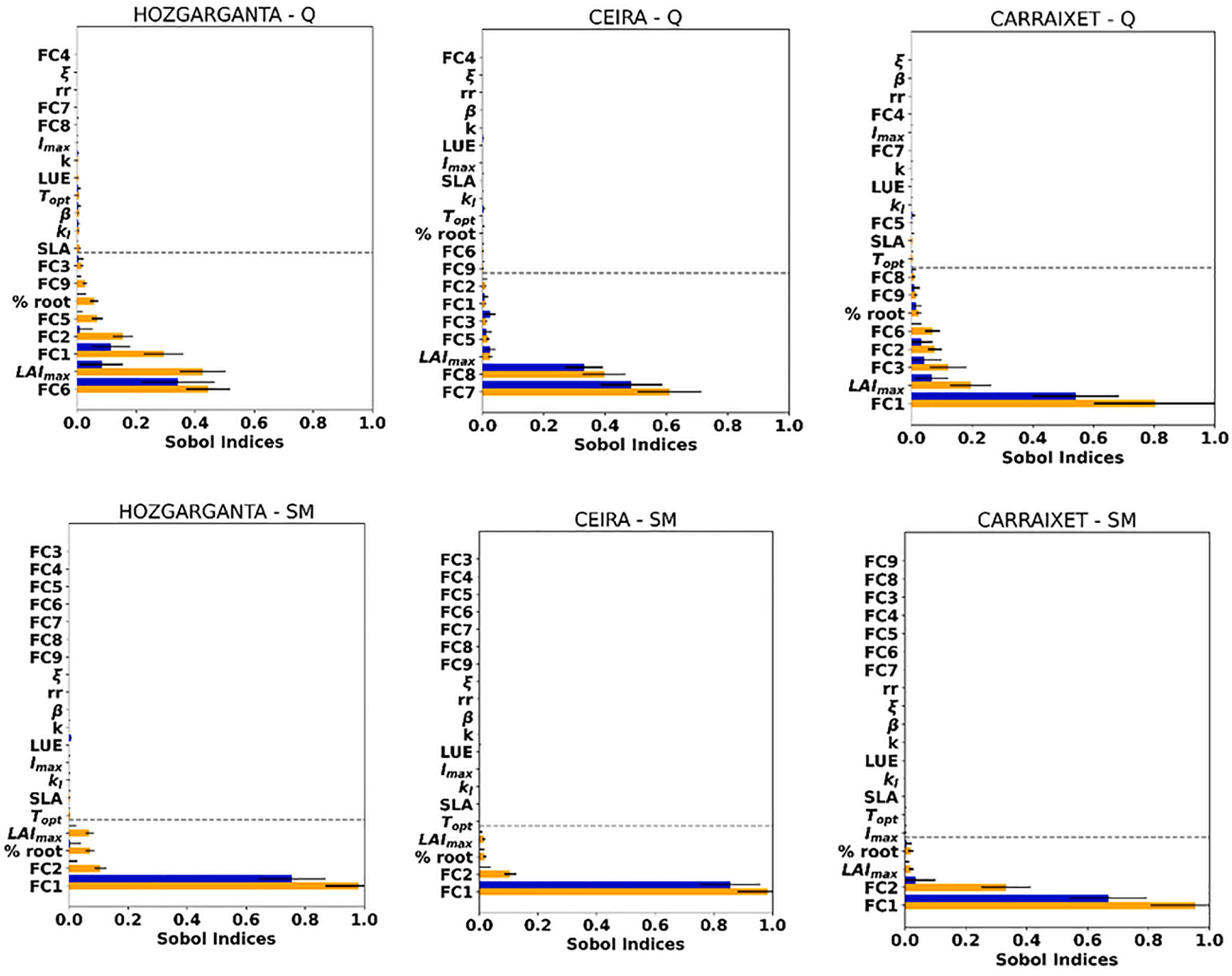

Fig. 4. Sobol sensitivity analysis for the 3 basins considered. Upper row refers to discharge results while lower row to the soil moisture. Sobol's first and total indices are displayed in blue and orange, respectively. (For interpretation of the references to colour in this figure legend, the reader is referred to the web version of this article.)

Table 4
Calibration parameters ranges for the case studies.

	Hozgarganta	Ceira	Carraixet
FC1	[0.8–1.3]	[1.2–1.5]	[1.3–1.6]
FC2	[0.6–1.3]	[0.6–1.3]	[1.0–1.3]
FC3	[0.2–0.8]	[0.2–0.8]	[0.2–0.6]
FC4	1	1	1
FC5	[0.2–0.8]	[0.2–0.8]	0.3
FC6	[1500–3000]	1000	[0.2–10]
FC7	0.2	[0.2–1]	0.2
FC8	1000	[4000–5000]	[100–500]
FC9	[0.1–0.6]	1	[0.05–0.15]
%root	0.1–0.4	0.1–0.4	0.1–0.4
LAI_{max}	0.7–5	0.7–5	0.7–5

digital elevation to correct the LST data for topographic effects. A more detailed description of the disaggregation methodology can be found in (Merlin et al., 2013). Same pre-processing of the final soil moisture values as the previous cases was considered. In this case, only days in which the downscaling was completely successful (i.e. proper reproduction of the 1 km spatial features) were considered. These products will be named from here on as SMAP-DPAT and SMOS-DPAT.

4. Methods

4.1. Surface soil moisture products comparison

Comparison of the products was performed both temporally and spatially. Temporal agreement amongst products was assessed using

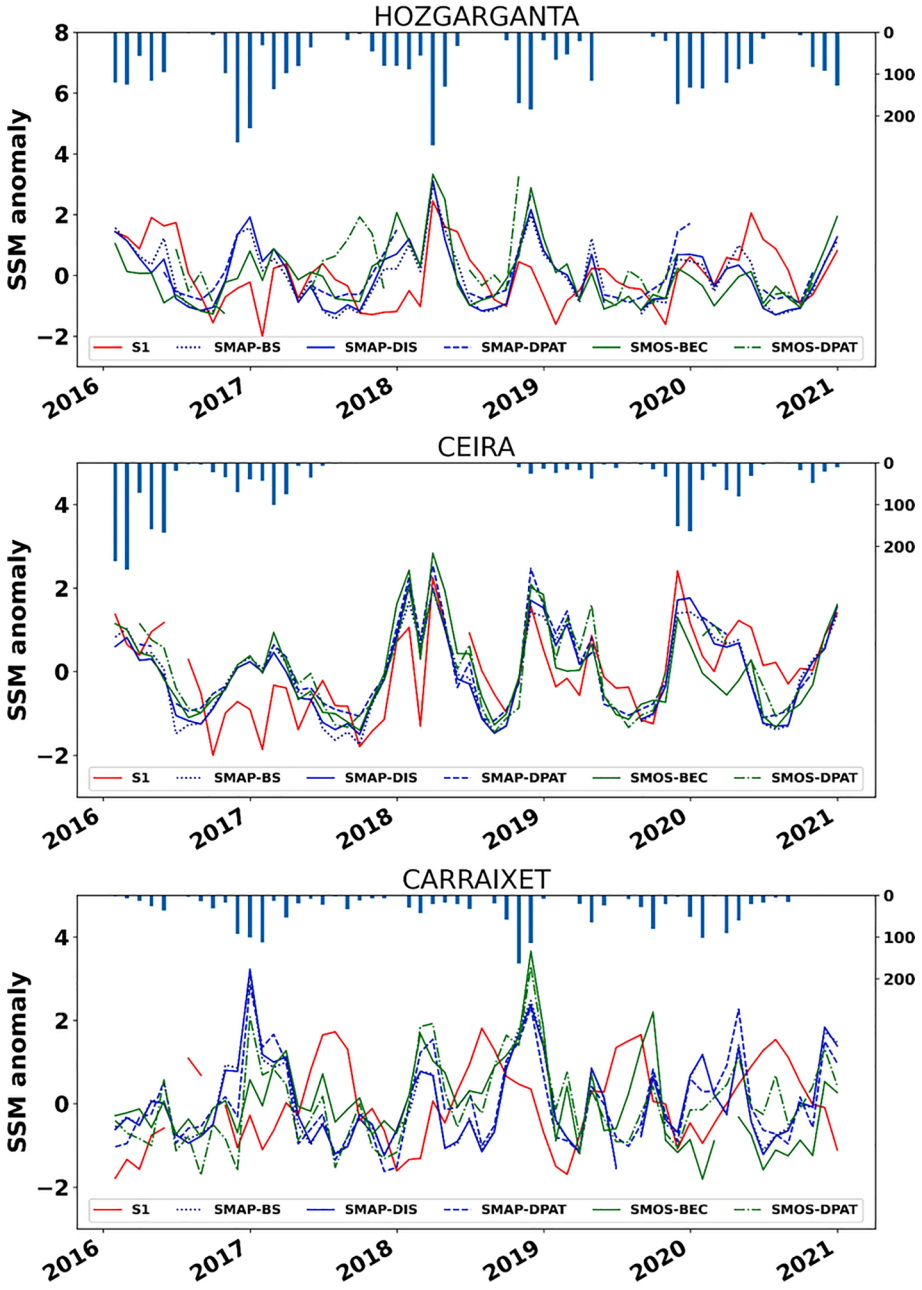

Fig. 5. Temporal evolution of the standardized monthly values for the different soil moisture products considered. Upper, middle and lower row refer to Hozgarganta, Ceira and Carraixet, respectively. Monthly aggregated precipitation values are also displayed. For the case of Hozgarganta, 03–2018 precipitation value was truncated for a better visualization and for Ceira, the period 08–2017 to 08–2018 has no precipitation records.

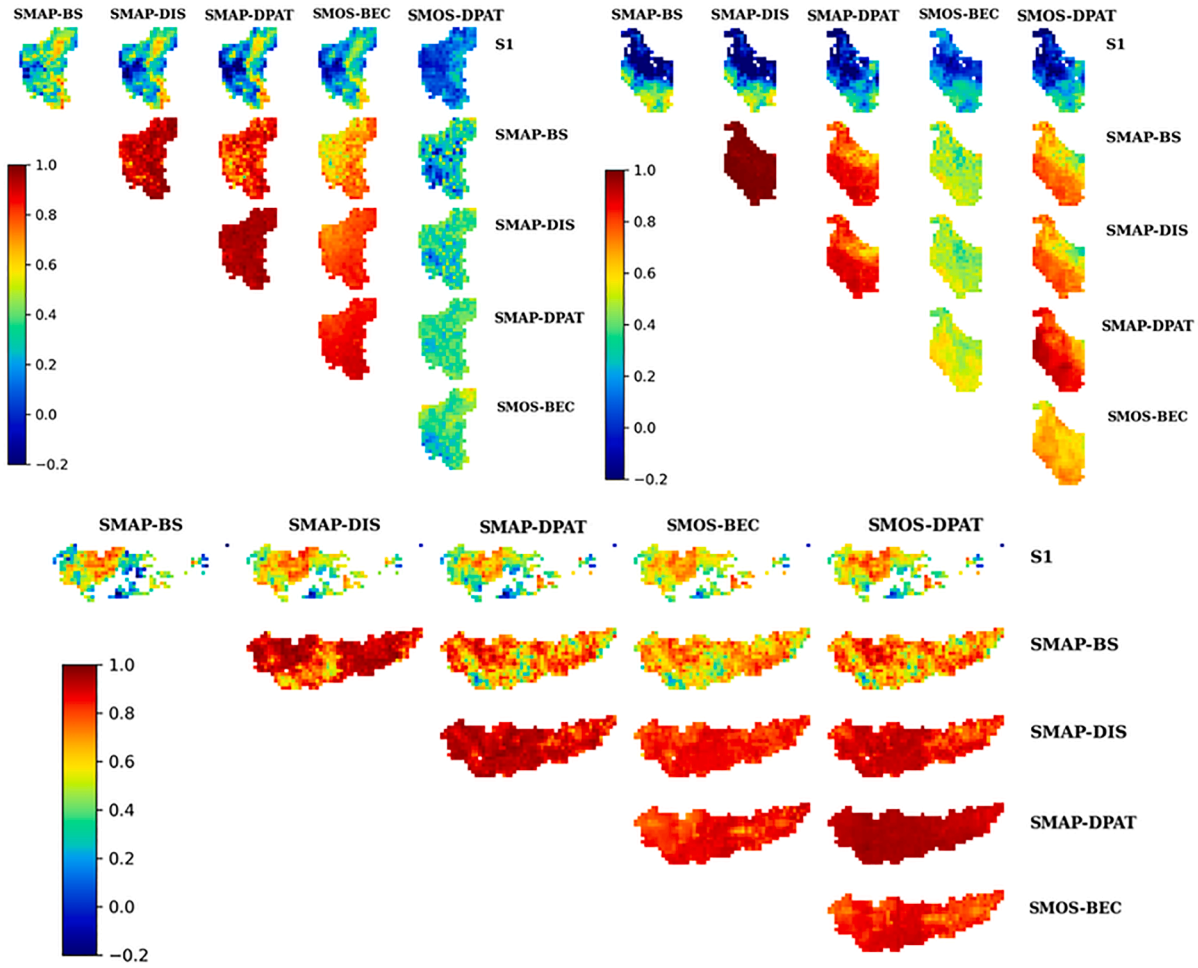

Fig. 6. Temporal correlation coefficient (R values) of the different soil moisture products for the three basins considered. Correlation coefficients were calculated considering standardized values.

series of aggregated at basin level soil moisture values and spatially distributed correlation images. SSM values were normalized using temporal Z-scores (period 2016-2020) in order to discard existing biases amongst products and make them comparable. . Finally, spatial pattern agreement was obtained by visual comparison of spatial Z-score SSM images. These scores were calculated based on spatial mean and standard deviation of the mean SSM image (period 2016–2020).

4.2. Model calibration

4.2.1. Sensitivity analysis

Prior to model calibration we performed a Sobol sensitivity analysis (Sobol et al., 2001; Saltelli et al., 2002-2010) that ranked which parameters were more significant to model performance and allowed us to reduce the number of parameters to calibrate. This method is based on an analysis of variance decomposition. It can be applied to non-linear models as no assumption between model input and output is required. Assuming that all model inputs are independent, output model variance can be decomposed into component variances from individuals and their interactions. The sensitivity of a single parameter or their interaction can be assessed by the percentage contribution to the total variance. These percentages are the so called Sobol's sensitivity indices. Sobol's first index correspond to the independent contribution of the input variables, Sobol's second index to the interaction among inputs variables and Sobol's total index correspond to the gathering of these two effects. This technique has been widely used for parameters sensitivity analysis in hydrological models (Song et al., 2015), providing an in-depth understanding of hydrological processes (Zhang et al., 2013). Main drawback is the high computational intensity associated requiring $nx(2m+2)$ model evaluations if second order effects are included (Herman & Usher, 2017) where n are the samples and m the model parameters. For a more detailed mathematical description, we refer to original works describing the method (Sobol et al., 2001; Saltelli et al., 2002-2010) and recent reviews for sensitivity analysis in hydrological modelling (Song et al., 2015).

For this study, in order to minimize the associated computational cost while still preserving representativeness of the results, Sobol analysis was applied over a semi-lumped version of the model (i.e. natural land uses, which are the ones to be calibrated, were considered to share same vegetation parameters while urban and agricultural land uses corresponding parameters were previously fixed to reference values). This approach substantially reduced the number of parameters in the analysis (9 hydrological parameters + 11 vegetation parameters). Sensitivity analysis was performed separately considering for streamflow and surface soil moisture. Nash-Sutcliffe efficiency index (Equation (3)) was used as the standard error metric in both cases. For streamflow, NSE was evaluated against discharge observations, while for SSM mean simulated values (considering the natural land uses for aggregation) were considered for model deviation assessment. Sensitivity analysis was performed over the calibration period. Sample size for the analysis was fixed at 500 corresponding to 21,000 model evaluations. Initial tests ensured the convergence of these results. Sensitivity parameters and

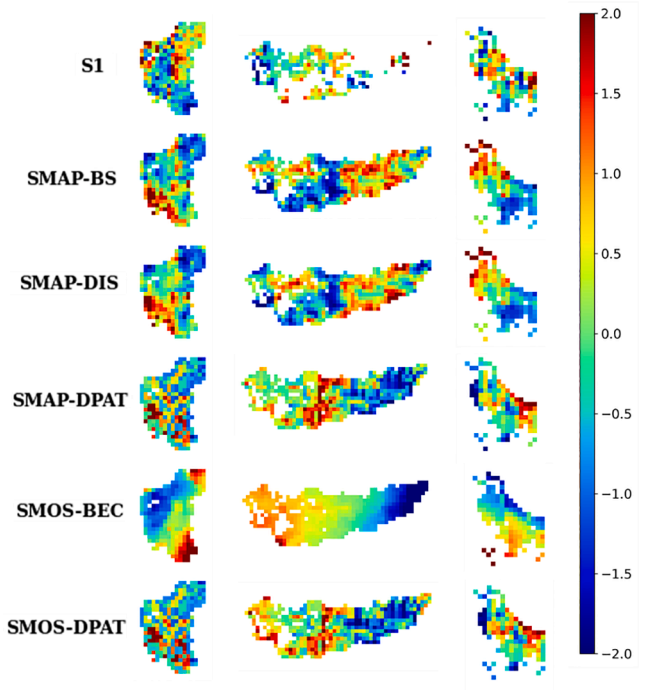

Fig. 7. Soil moisture spatial anomalies for the different soil moisture products and basins considered. Displayed are the spatial standardized anomalies in the range [-2, 2].

associated lower and upper bounds are summarized in Table 3. They were based on previous works using TETIS eco-hydrological model (Ruiz-Pérez et al., 2017; Puertes et al., 2019; Echeverría et al., 2019), manually refined to ensure a good performance of the model during the analysis. All the calculations were performed using the Python SALib toolbox (Herman & Usher, 2017).

In Fig. 4, Sobol's sensitivity analysis indices are displayed. A threshold of 1% (dotted line) was considered for discriminating between sensitive and insensitive parameters (Tang et al., 2007). Several conclusions can be derived from Fig. 4: 1) regarding vegetation sub-model % roots and Lai_{max} can be considered as the most sensitive parameters (for both SSM and Q). It can be deduced that LAI can be more influent than some hydrological parameters in the proper representation of the discharge. 2) regarding hydrological sub-model, different sensitive parameters were found for the different basins considered according to their hydrological characteristics. For Hozgarganta, we observed that a more important contribution of the interflow followed by direct runoff. In Ceira, an accurate baseflow description in the model becomes important for the reproduction of observed values. For Carraixet, direct runoff is the major contribution to the observed streamflow, followed by interflow.

4.2.2. *Calibrations experiments and assessment metrics*

The initial parameters range values were established by screening the simulations performed during the sensitivity analysis (NSE values greater than 0.5). Calibration parameters and associated ranges are summarized in Table 4. For the case of % roots and Lai_{max} parameters they were calibrated specifically for each of the natural land uses considered. These are according to the Corine classification: broad-leaved forests, mixed forests, coniferous forests, natural grasslands, moors and heathland, sclerophyllous vegetation, transitional woodland-shrub and sparsely vegetated areas. For the rest of the vegetation parameters, they were fixed according to previous values of the literature. T_{opt} was fixed at 18 °C according to Ruiz-Perez et al., 2017. Respiration ratio was fixed to a value of 0.066 (gC/gNd) according to Bonan et al., 2003. K_{decay} was fixed to 0.56 according to the values provided by Zhang et al., 2014. From Montaldo et al., 2005, senescence factor was fixed in the range from 0.008 to 0.004 (value of 0.006 in that study) adequating to the different land uses. LUE values were obtained from the Copernicus Dry Matter Productivity ATBD and SLA values from Heinsch et al., 2003. I_{max} was fixed to a value of 0.2 according to Manfreda et al. (2005).

Considering the hydrological and vegetation parameters a total of 22, 16 and 16 parameters were to be calibrated for the cases of Hozgarganta, Ceira and Carraixet respectively. For Hozgarganta and Carraixet, calibration period was 2016–2017 and validation period was 2018–2019. For the case of Ceira, calibration period was 08–2015 to 07–2017 and validation period 03–2019 to 07–2020. Approximately an additional year (7 months for the case of Ceira) was considered for model warm-up before calibration for each of the basins considered. Calibration was performed based on a multi-objective approach using the Multiobjective Shuffled Complex Evolution Metropolis (MOSCEM-UA) algorithm (Vrugt et al., 2003a) considering discharge (Q) and

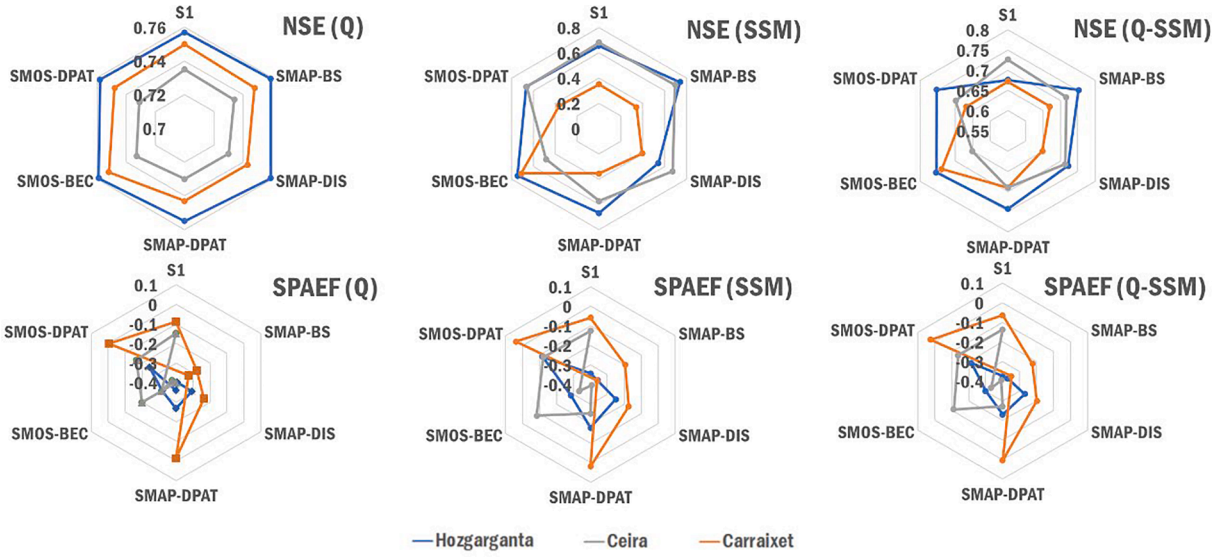

Fig. 8. Calibration NSE and SPAEF values for the three pareto points selected (Q, SSM and Q-SSM) and for the different basins considered.

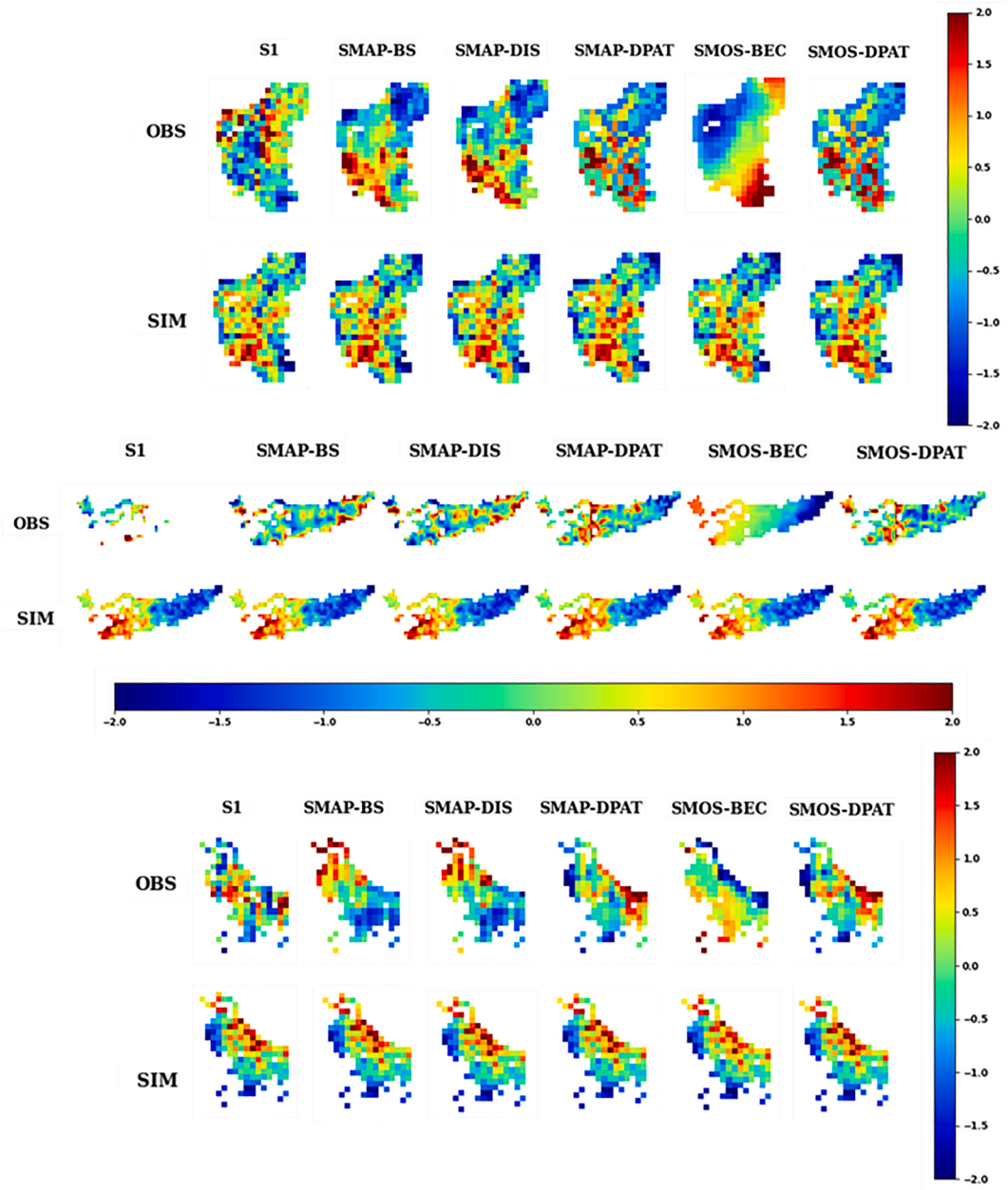

Fig. 9. Spatial patterns for the calibration period for the cases of study (Q-SSM-case). Displayed are the spatial standardized anomalies in the range [-2, 2].

surface soil moisture (SSM) observations. The MOSCEM-UA algorithm combines the strengths of the complex evolution' used in the Shuffle Complex Evolutionary (SCE-UA) algorithm (Duan et al., 1992) and the probabilistic search method known as covariance-annealing used in Shuffled Complex Evolution Metropolis (SCEM-UA) (Vrugt et al., 2003b) together with and improved version of the assignment method aptitude (Zitzler and Thiele, 1999) to determine an efficient estimate of the Pareto frontier. For this study the initial population was obtained as the product of the number of complexes (for this study 10 complexes were selected) and 2*nvar + 1 (being nvar the number of variables). Scale factor (β) and L (number of new candidates in each complex) were obtained following Vrugt et al., 2003a. Number of iterations were set so that at least 5000 function evaluations were performed. Objective functions were the NSE [-∞,1] for discharge while the Spatial Efficiency Metric (SPAEF) [-∞,1] (Koch et al., 2018) for the evaluation of the spatial agreement between the remote sensing-based soil moisture observations and TETIS soil moisture simulations. SPAEF is bias insensitive and focused only on spatial patterns (Demirel et al., 2018). These metrics are provided in Equations (3) and (4).

$$NSE = 1 - \frac{\sum_{i=1}^{n}(Q_{si} - Q_{oi})}{\sum_{i=1}^{n}(Q_{oi} - \overline{Q_o})} \tag{3}$$

where Q_s and Q_O are the simulated and observed flows on day i, n is the total number of days and $\overline{Q_o}$ is the mean daily measured flow for the analysed period.

$$SPAEF = 1 - \sqrt{(\alpha - 1)^2 + (\beta - 1)^2 + (\gamma - 1)^2} \tag{4}$$

where α is the Pearson correlation coefficient ($\rho(A,B)$ between the observed SSM map (A) and simulated SSM map (B) for a particular month, β is the fraction of coefficient of variations representing spatial variability and γ is the percentage of histogram intersection. This calculation is performed after normalization of the observed and simu-

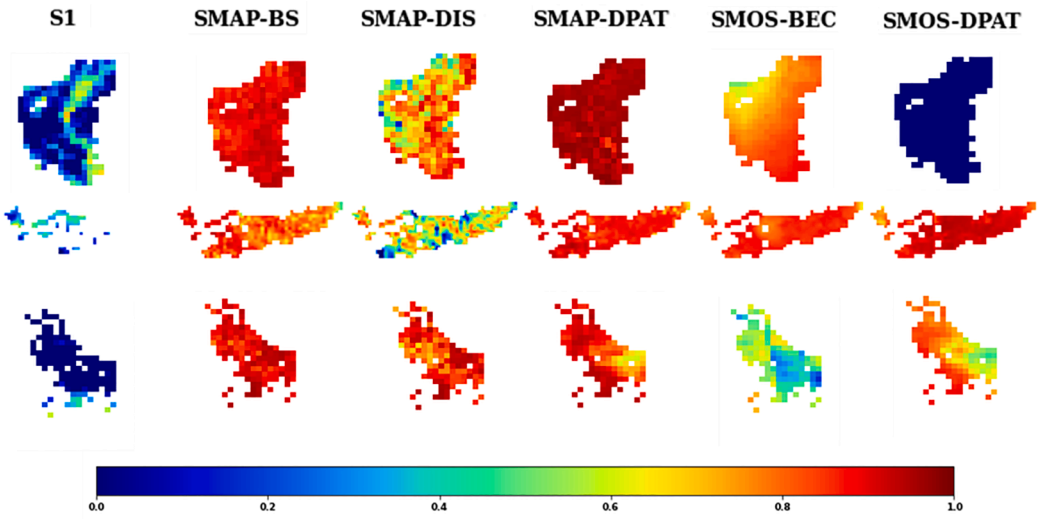

Fig. 10. Temporal correlation coefficient (R value) of observed estimates against TETIS simulations for the calibration period (Q-SSM-case). They are displayed in the range [0,1] for a better visualization.

lated maps using z-scores (i.e. mean equal to 0 and standard deviation equal to 1). For each particular image (i.e. month) a SPAEF value was obtained. The mean value of these scores was considered as representative of the corresponding time series.

The multi-objective calibration was performed for all the products considered and for the study cases. As the adjustment for Q and SSM is different amongst the non-dominated solutions, we selected for posterior analysis three solution candidates: best performance in Q (Q-case), best performance in SSM (SSM-case) and a compromise solution in the performance of both Q and SM (Q-SSM-case). The first two points were selected by seeking for the point in the pareto frontier that maximises the corresponding objective functions (i.e. NSE for Q and SPAEF for SSM). The third point was the one with minimum Euclidean distance to the reference point. This reference point is obtained considering the best objective value for each of the two objectives functions. Previous to distance calculation, these objective function values were normalized between the maximum and minimum values respectively.

4.3. Model evaluation

Evaluation of the different experiments (Q-case, SSM-case and Q-SSM-case) was performed by quantitative analysis of NSE and SPAEF metrics. In addition, for Q-SSM-case, spatial patterns are provided for a visual assessment of the agreement between simulated and observed SSM. Series aggregated at basin level and spatially distributed correlation maps allowed the comparison of the temporal dynamics of SSM.

5. Results

5.1. RS soil moisture inter-comparison

Fig. 5 shows the temporal dynamics of the soil moisture products considered over the respective basins. Values were calculated considering natural land uses (i.e. no irrigation). Fig. 6 displays the spatially distributed correlation coefficient images, for completeness they were calculated over the whole basin area.

It is clearly observed (Fig. 5) that for the three cases of study, Ceira is the one in which a clear temporal agreement between the different soil moisture products exists. Most discrepant product is S1, which also reproduces a discrepant behaviour for the other two study cases. The temporal evolution showed some negative (08–2016 till 12–2019) and positive (year 2020) bias in S1 for this study case. In addition, the temporal correlation coefficient for S1 ranges between −0.2 to 0.8, while the rest of the cases yield values in the range 0.8–1.0 (Fig. 6). Nevertheless, all products represent the corresponding monthly rain events (period 08–2017 to 08–2018 has no precipitation records) (Fig. 5). In the case of Hozgarganta, main discrepancies arise also for S1 product that still shows some clear bias and SMOS-DPAT product, with a positive value in 2017 that do not relate to the observed precipitation (Fig. 5). The temporal correlation coefficient for S1/SMOS-DPAT ranges between −0.2 to 0.8/0.6 respectively,while the rest of the cases yield values in the range 0.8–1.0 (Fig. 6). The SSM temporal evolution clearly follows the precipitation evolution (Fig. 5). For Carraixet, main discrepant temporal evolutions are S1 and SMOS-BEC. For S1, a clear bias is observed. In addition, it does not follow precipitation monthly amounts (2018, 2019 and 2020). Fig. 6 shows S1 correlation coefficient values in the range of −0.2 to 0.6. It is worth highlighting that this poor performance is related to land uses. While inconsistencies were observed for the forest and natural land uses (upper part of the basin) they have been found less evident for the agriculture uses (lower part of the basin).

Fig. 7 displays the spatial patterns that refer to the standardized spatial anomalies of the mean values for the period 2016–2020. Spatial patterns matched for products that share the same disaggregating methodology. This fact is reproduced for the three cases of study. For Hozgarganta, SMAP-DIS and SMAP-BS share a similar spatial pattern while also for the case of SMAP-DPAT and SMOS-DPAT. SMOS-BEC provides the most discrepant spatial pattern amongst products. For Ceira, SMAP-DIS/SMAP-BS, SMAP-DPAT/SMOS-DPAT/S1 show a comparable behaviour, respectively. SMOS-BEC shares a more similar pattern to this last one group For Carraixet, same behaviour as in Ceira is reproduced, in exception of SMOS-BEC.

5.2. Model performance for the different soil moisture products

5.2.1. Calibration

Fig. 8 displays the calibration results for the study cases (values are summarized in Table S1 of supplementary material). Q is well represented in every case analysed. Only exception was found in the analysis of some products in Carraixet for the SSM-case (NSE < 0.4) and Ceira-SMOS-BEC for the SSM-case (NSE < 0.5). Q-case provided the best NSE values in every case study, although Q-SSM-case raised comparable results (NSE 0.65–0.75). SSM-case showed the best SPAEF values with slight differences comparing to other approaches. However, SPAEF values can provide maximum deviations greater than 0.45 for the different product combinations and study cases. This fact indicates that the spatial agreement between the soil moisture products and the model

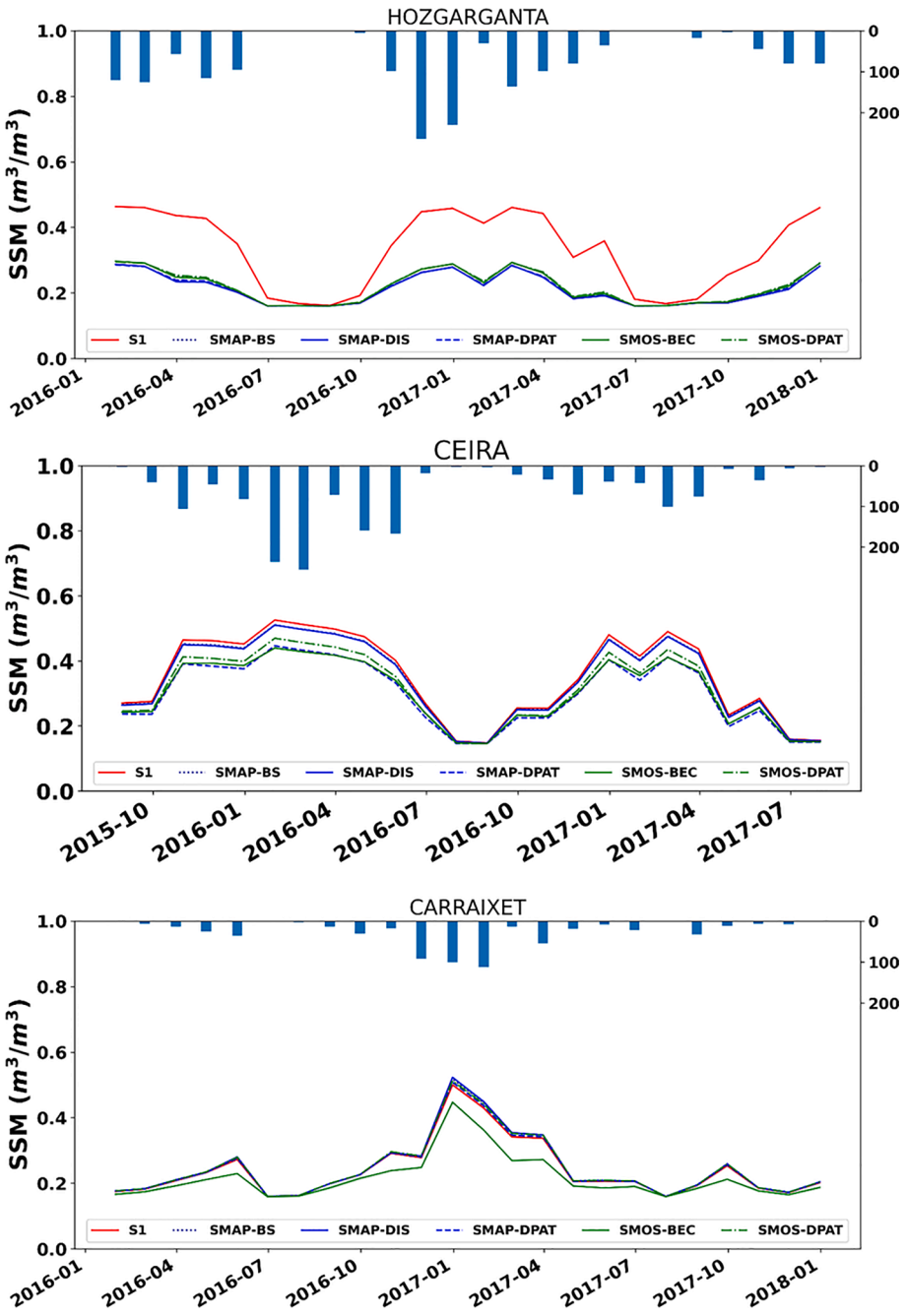

Fig. 11. Temporal evolution in the calibration period of the monthly TETIS SSM predictions for the different configurations considered (Q-SSM-case).

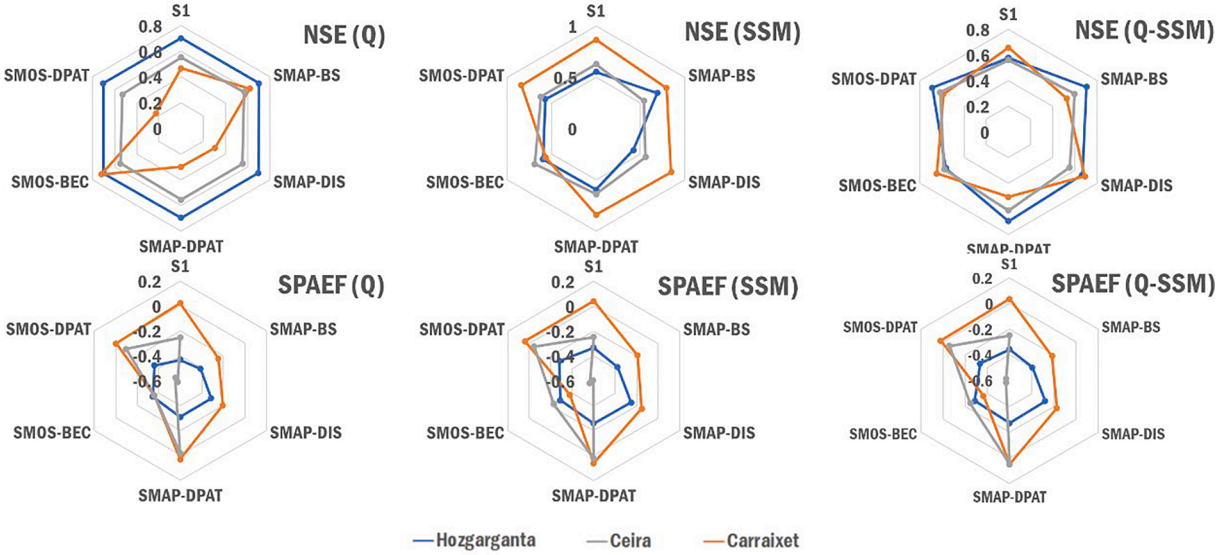

Fig. 12. Validation NSE and SPAEF values for the three pareto points selected (Q, SSM and Q-SSM) and for the different basins considered.

simulations will become more determinant in the selection of the best performing combinations than the NSE. Carraixet is clearly the one in which TETIS provides a major spatial agreement, followed by Ceira and Hozgarganta. Focusing on the comparison of the different product combinations for each of the study case, we observe that for Hozgarganta, SMOS-DPAT followed closely by SMAP-DPAT provides the best SPAEF values for all the cases (Q (-0.243), SSM (-0.117) and Q-SSM (-0.215)). SMOS-BEC and SMAP-DIS provide a similar performance (ranging from −0.250 to −0.318 in every cases) while SMAP-BS and S1 provide the worst performance (SPAEF lower than −0.340 in every case). For Ceira, SMAP-BS and SMAP-DIS are the worst ranking in SPAEF values (values lower than −0.4). S1, SMOS-BEC, SMOS-DPAT and SMAP-DPAT provide a better performance. In the Q-SSM case, S1 ranks the best in NSE (value of 0.726) while SMOS-BEC ranks the best in SPAEF (value of −0.112). SMOS-DPAT, however ranks better than SMOS-BEC in NSE while still having closer SPAEF values (-0.137). SMAP-DPAT is the one amongst these four that provides the worst performance in SPAEF. For Carraixet, SMOS-BEC provides a different behaviour. It always provides worst performing SPAEF values for the three cases, thus indicating that TETIS is never able to reproduce the associated spatial patterns. For the rest of the products, S1, SMAP-DPAT and SMOS-DPAT rank the best in terms of spatial agreement.

Fig. 9 displays the spatial patterns for the calibration period (Q-SSM-case). SMAP-DPAT and SMOS-DPAT showed the major agreement for Hozgarganta, Ceira and Carraixet. In addition, S1 works properly for Ceira and Carraixet, although the number of available pixels in Ceira is not significant to state the agreement. SMOS-BEC must be highlighted in the case of Ceira. Similar main spatial patterns were provided by TETIS for the reference products. Transitional pixels between the main different areas of the standardized anomalies were highly affected by the reference product considered in the calibration process, in exception of Carraixet in which the main spatial patterns are best fitting the reference product.

Fig. 10 shows the correlation coefficient maps (Q-SSM-case). TETIS simulations provide the worst agreement with S1 for all the study cases and SMOS-DPAT for Hozgarganta. Other cases have correlation coefficient values greater than 0.8, thus indicating the temporal agreement. Exceptions are SMAP-DIS for Ceira and Hozgarganta and SMOS-BEC for Carraixet with correlation values between 0.2 and 0.8. Temporal evolution of SSM were coherent to precipitations in every case study (Fig. 11). Differences between reference products were observed only in terms of absolute SSM values.

5.2.2. Validation

Fig. 12 displays the validation results for the three case studies (values are summarized in Table S2 of supplementary material). TETIS tends to provide a worse performance during the validation phase than during the calibration phase. Only cases in which this is not accomplished are SSM-case for Ceira (SMAP-DPAT, SMOS-BEC) and Carraixet (all products in exception of SMOS-BEC). For Carraixet, calibrating the model in order to adjust to only one variable will result in an improper performance. While NSE values in the calibrating phase (Fig. 8) are acceptable they are not able to reproduce the validation observations (Fig. 12). On the contrary, adjusting only to SSM provides an unacceptable performance in calibration (NSE < 0.4) while a surprisingly good performance during validation. These results indicated that the inclusion of SSM in a multi-objective calibration increased the model capability to reproduce not only the SSM spatial patterns but also the Q in different hydrologic periods. Considering the Q-SSM-case , for all the study cases and products combinations NSE > 0.5 is provided. Calibrations and validation NSE values are also in agreement. This indicates that all the combinations provide a realistic description of the discharge and therefore supporting the validity of the multi-objective calibration approach.

Moving to each study case comparison, for Hozgarganta the calibration candidate's combinations SMAP-DPAT and SMOS-DPAT provide NSE values > 0.65, being SMAP-DPAT the best option in terms of SPAEF with slight differences with the rest of the products. However, SPAEF values are lower than −0.2 thus preventing to state the agreement between the models estimates and products observations. In consequence, no particular product can be highlighted for its performance in both Q and SSM in the Hozgarganta study case. Moving to Ceira, again SMAP-DPAT and SMOS-DPAT provide the best performance in both NSE and SPAEF. Although S1 and SMOS-BEC still provided acceptable results in terms of NSE, the spatial performance was worse (SPAEF $<$ -0.2). SMOS-DPAT is preferred because of the good performance in both calibration and validation periods. Finally, for Carraixet, S1, SMAP-DPAT and SMOS-DPAT provided good performance in both NSE and SPAEF. It is remarkably that S1 actually provided the best NSE metric, in spite of the unrealistic temporal behaviour observed, followed closely by SMOS-DPAT and SMAP-DPAT.

Fig. 13 displays the spatial patterns for the validation period (Q-SSM-case). Results are analogous to the calibration period. SMAP-DPAT and SMOS-DPAT still provided the best agreement in all the case studies, with S1 performing particularly well also in Carraixet. Fig. 14 shows the

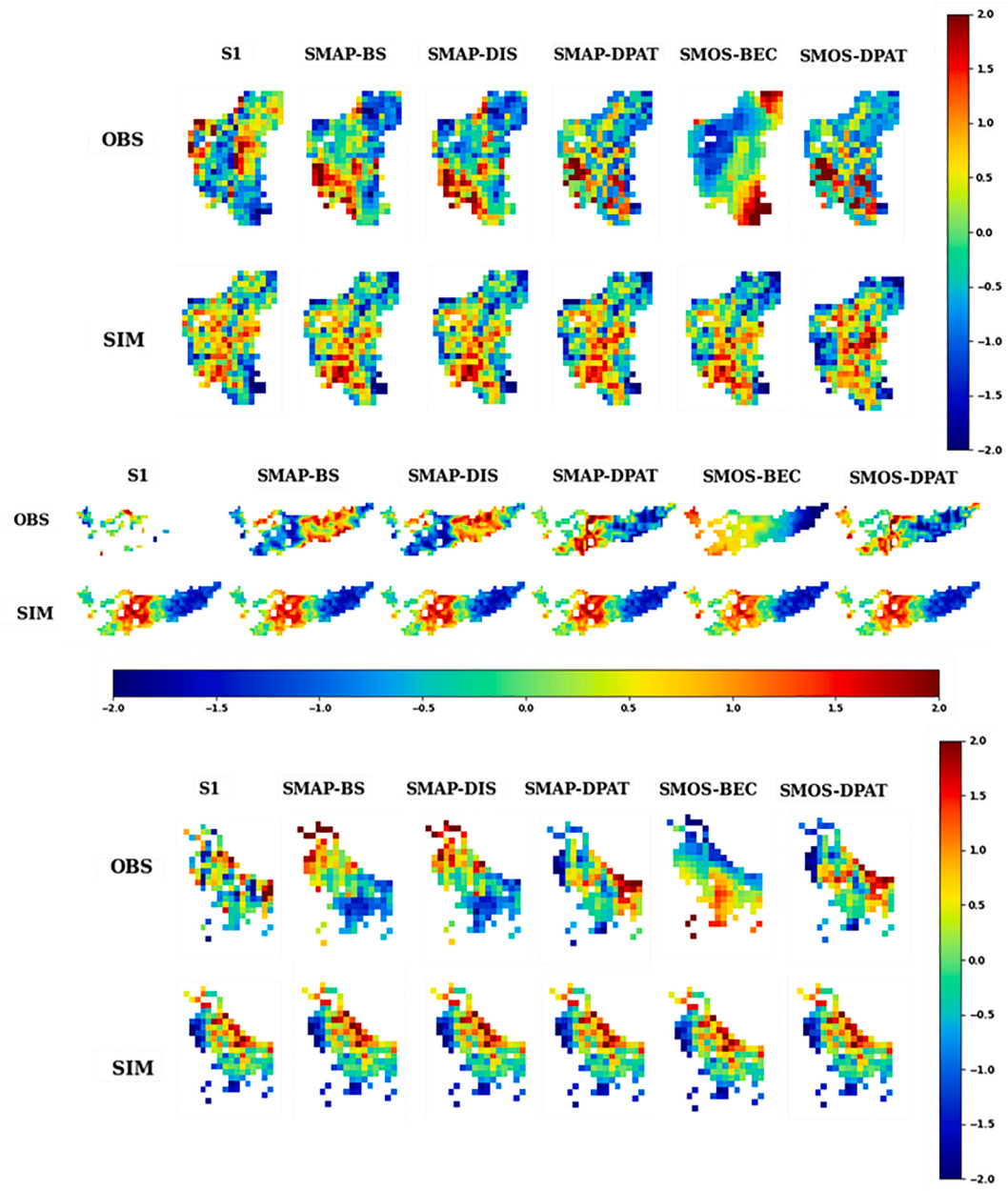

Fig. 13. Spatial patterns for the validation period for the cases of study (Q-SSM-case). Displayed are the spatial standardized anomalies in the range [-2, 2].

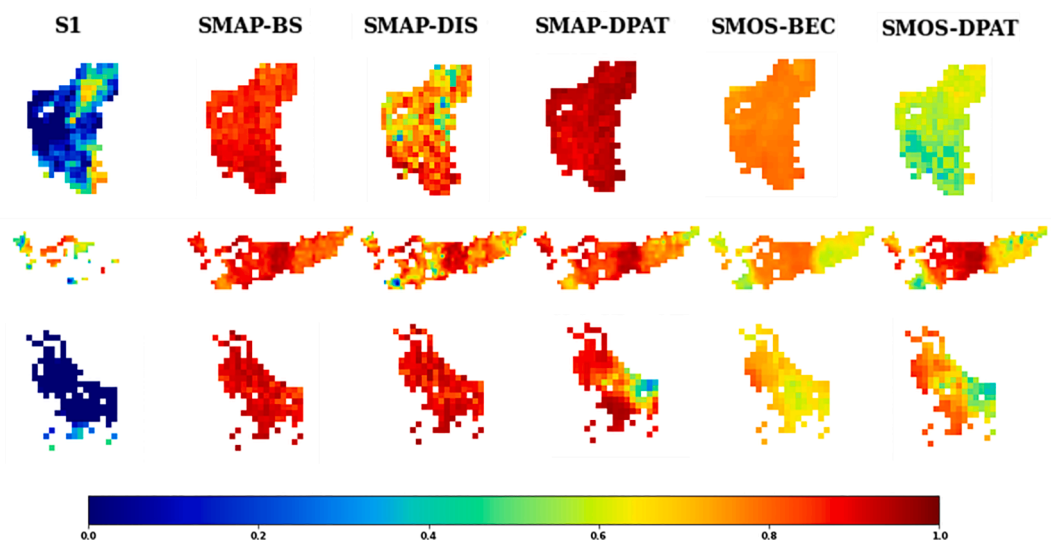

Fig. 14. Temporal correlation coefficient (R value) of observed estimates against TETIS simulations for the validation period (Q-SSM-case). They are displayed in the range [0,1] for a better visualization.

correlation coefficient maps. S1 again provided the worst temporal agreement with a slight improvement in Ceira. The rest of the combinations provided correlation values over 0.5 with SMAP products best fitting. Finally, the SSM temporal evolution in this period (Fig. 15) again is coherent to precipitations in every case study, still showing main differences in terms of absolute SSM values.

6. Discussion

Coarse spatial resolution of satellite SSM (SMAP and SMOS) estimates products have only provided the opportunity of considering the temporal dynamic of the SSM variable when regional studies of hydrological implementation were approached. Since the existing downscaling methods (Piles et al., 2011; Piles et al., 2012; Merlin et al., 2013) provide increased spatial resolutions in addition to new sensor estimates (Bauer-Marschallinger et al., 2019), we postulate that the inclusion of spatial patterns in the implementation of hydrological models may improve their performance. There is a lack of testing the improved spatial information of these downscaled products in small basins, specifically in the Mediterranean region. This study evaluates the suitability of several 1 km spatial SSM estimates (S1, SMAP-BS, SMAP-DIS, SMOS-BEC, SMAP-DPAT, SMOS-DPAT) for this purpose. As first step, a comparison of the available products is required. We observed that the agreement among the spatial and temporal dynamics of the evaluated products is not as good as expected. The suitability of hydrological distributed models for the reproduction of main hydrological state variables have already been demonstrated (Ruiz-Pérez et al 2016; Ruiz-Pérez et al., 2017; Puertes et al., 2019; Echeverría et al., 2019; Barrientos et al 2020). Thus, we can consider these models as validation tools to test the performance of the available comparable products. Particularly, the TETIS conceptual model has demonstrated to be a good choice for this purpose (Echeverría et al., 2019). This paper encompasses: first, the multi-objective and multi-variable calibration of the model considering previously described SSM products; second, the analysis of Pareto frontiers in terms of temporal dynamics of streamflow, spatial agreement of SSM, and both; finally, the performance comparison amongst the different products. Despite the significant differences amongst SSM products, results showed an improvement when the SSM spatial patterns were considered in the calibration process. We observed that not all the products have the same agreement with TETIS results.

In the comparison of the SSM products, we observed a relative temporal agreement in exception of S1 that has different temporal dynamics. This product showed a strong overestimation of the SSM during dry months in Carraixet. Previous studies (Escorihuela and Quintana-Seguí, 2016) pointed out that in semi-arid regions the artificial increase in soil moisture can be the result of the increase in the effective soil roughness due to volume scattering. This poor performance can be also associated to different factors. Firstly, S1 retrieval algorithm does not consider vegetation dynamics on radar backscatter signal thus leading to potential biases during vegetation full development (Bauer-Marschallinger et al., 2019). In addition, the sensitivity of the C-band backscatter is likely to be reduced in high density vegetated areas with leaf area index larger than 0.6 (Ohja et al., 2021). The temporal agreement between products is higher in Ceira than the other two basins. The location of the study sites may have influence in the SSM retrieval. Although the three basins share some issues in the soil moisture retrieval (topography, dense vegetation), it is true that Ceira is in an easier to solve area for the retrieval. Carraixet is close to the coast, thus some noise can affect due to sea-land disturbance. Water areas present near Hozgarganta can also disfavour the SSM retrieval. Nevertheless, in spite of some exceptions (S1 and SMOS-DPAT for Hozgarganta) all the products generally agree in their temporal dynamics (correlation coefficient greater than 0.4 in Fig. 6). Portal et al., 2020, performed a comparison between SMAP and SMOS products over the Iberian Peninsula, and they observed the same general temporal agreement. In this study, they also pointed out that the methodology employed for the downscaling depend on the scale information the SSM products employed (S1 radar backscatter, LST, NDVI, land use). We observe this same conclusion for the products considered. Fig. 7, shows that for spatial patterns the disaggregating methodology employed is more relevant than the sensor (i.e. SMOS, SMAP, S1).

Traditional approaches consider only streamflow information in the calibration process. Considering another state variable as unique objective function does not prevent the problem of equifinality. Therefore, to follow a multi-objective approach is recommended (Dembelé

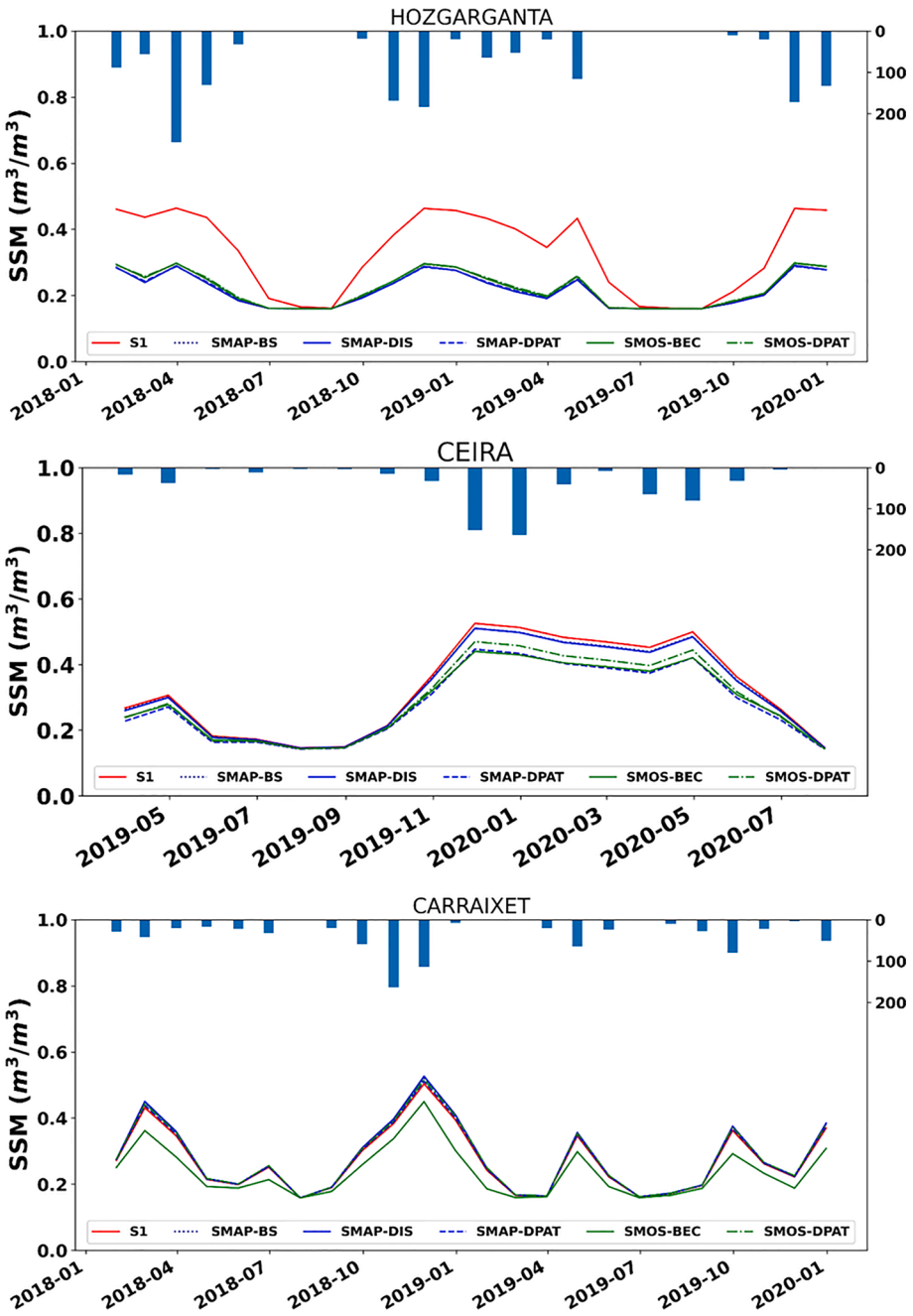

Fig. 15. Temporal evolution in the validation period of the monthly TETIS SSM predictions for the different configurations considered (Q-SSM-case).

et al., 2020b). Although calibrating considering separately in Q and SSM will result in good implementations, we decided to compare their effect in the pareto frontier. Selecting the best performing non-dominated solutions in terms of Q and SSM gave us an idea of their relevance in a comparable context. Comparing the calibration and validation phases we found that the model conducted more robustly when both Q and SSM information was considered through the selection of an optimum non-dominated solution. Particularly, intermittent streams such as Carraixet will improve the adjustment of its hydrology (i.e. SSM patterns) through this approach during dry periods in which Q is not enough representative. This fact was advanced by the sensitivity analysis (Fig. 4) where correction factor related to the static storage (FC1) was the most relevant.

The spatial pattern of the precipitation intensely determines the SSM spatial patterns offered by the model. Thus, the calibration considering different SSM reference products introduced variations limited to transitional areas between homologous main spatial patterns. This endorses the fact that using physically based models is a good criterion to validate satellite products. The dependency on the calibration and validation periods is expected to be additionally high. Nevertheless, we cannot test this hypothesis since the SSM observed data is limited mostly to the period from 2015 to present. SPAEF results are frequently negative or mostly nulls similar to other authors (i.e. Dembelé et al, 2020a). These evidence possible causes: incoherencies in the SSM retrieval, lack of representativity in spatial resolution, temporal limitations of satellite products, and/or differences in input data generation. The influence of land use has been reported by Burgin et al. (2017) and soil hydraulic properties has been previously reported by (Baroni et al., 2010, Livneh et al., 2015; Ayana et al., 2019). SMAP-DPAT and SMOS-DPAT were the products that provided better spatial agreement to the TETIS outputs.

Additionally, S1 provided remarkable agreement in Carraixet. In Ceira case study, we cannot state the agreement to S1 since few pixels are available for comparison. Thus, to decide while S1 is useful in the Mediterranean region, other basins need to be evaluated. On the contrary, we can state that Lobelia products provide the best representation of the SSM spatial patterns in the selected case studies.

Limitations in this study open the door to future research. Higher spatial resolution, higher reliability of spatial products, and higher temporal coverage may lead to improved adjustments. Results can be model dependent; in consequence we encourage other models to be tested under this approach. Recently, new metrics for spatial pattern comparison have aroused (such as SPAEF), however this is still an active field of research. New metrics, algorithms and objective functions should be considered before performing similar analysis. Inclusion of spatial patterns from complementary state variables in multi-objective calibration efforts is challenging but it is expected to offer promising results (Dembelé et al., 2020a).

7. Conclusions

We explored the usefulness of eco-hydrological distributed modelling as a validation tool for remote sensing SSM products. This study provides a valuable advance in the filling of the existent gap in the validation of the spatial patterns of current SSM products. The study frame is the Mediterranean region in which three small basins were selected as representative case studies. Within this context, differences in temporal and spatial dynamics of the reference products were found. The multi-objective calibration approach proposed increased the robustness of the modelling despite the differences amongst products.

While SMAP-DPAT and SMOS-DPAT achieved the best agreement in terms of spatial and temporal representativeness, the other products showed some strengths. S1 did not provided a realistic temporal evolution. In contrast, the spatial patterns fitted correctly the distribution provided by TETIS model. Unfortunately, the data is not sufficient in all the basins. This is the case of Ceira. In Carraixet S1 agreement was comparable to SMAP-DPAT and SMOS-DPAT results. SMAP-BS and SMAP-DIS showed an opposite behaviour, with a good temporal representation but poor spatial representativeness for some specific cases. This is more evident in the case of Ceira. Finally, SMOS-BEC followed the line of SMAP-BS and SMAP-DIS, showing spatial disagreement between model simulations and observations.

Limitations of this study have been highlighted. Model dependency, uncertainties in SSM products, temporal calibration/validation periods restrictions (2015-present). Although results are dependent on the basin characteristics (case-specific) this paper provides evidence on the necessity to incorporate the spatial patterns information in the calibration of hydrological model

CRediT authorship contribution statement

José Gomis-Cebolla: Conceptualization, Methodology, Formal analysis, Writing – original draft, Writing – review & editing. **Alicia Garcia-Arias:** Conceptualization, Methodology, Formal analysis, Writing – original draft, Writing – review & editing. **Martí Perpinyà-Vallès:** Resources, Writing – review & editing. **Félix Francés:** Supervision, Project administration, Funding acquisition, Writing – review & editing.

Declaration of Competing Interest

The authors declare that they have no known competing financial interests or personal relationships that could have appeared to influence the work reported in this paper.

Acknowledgments

This study was founded by the Spanish AEI within the program WaterJPI through the project iAqueduct (PCI2019-103729), by the EC Life project ResilientForests (LIFE17 CCA/ES/000063), and by the project Water4Cast funded by Generalitat Valenciana (PROMETEO/2021/074). We also acknowledge the following hydrometeorological data providers institutions: SiAR, SAIH-HIDROSUR, SAIH Júcar and SNIRH.

Appendix A. Supplementary data

Supplementary data to this article can be found online at https://doi.org/10.1016/j.jhydrol.2022.127569.

References

Abbaszadeh, P., Gavahi, K., Moradkhani, H., 2020. Multivariate remotely sensed and in-situ data assimilation for enhancing community WRF-Hydro model forecasting. Adv. Water Resour. 145, 103721. https://doi.org/10.1016/j.advwatres.2020.103721.

Al-Yaari, A., Wigneron, J.-P., Dorigo, W., Colliander, A., Pellarin, T., Hahn, S., Mialon, A., Richaume, P., Fernandez-Moran, R., Fan, L., Kerr, Y.H., De Lannoy, G., 2019. Assessment and inter-comparison of recently developed/reprocessed microwave satellite soil moisture products using ISMN ground-based measurements. Remote Sens. Environ. 224, 289–303.

Alvarez-Garreton, C., Ryu, D., Western, A.W., Crow, W.T., Su, C.-H., Robertson, D.R., 2016. Dual assimilation of satellite soil moisture to improve streamflow prediction in data-scarce catchments. Water Resour. Res. 52 (7), 5357–5375.

Ayana, E.K., Dile, Y.T., Narasimhan, B., Srinivasan, R., 2019. Dividends in flow prediction improvement using high-resolution soil database. J. Hydrol.: Reg. Stud. 21, 159–175.

Bai, P., Liu, X., Zhang, Y., Liu, C., 2018. Incorporating vegetation dynamics noticeably improved performance of hydrological model under vegetation greening. Sci. Total Environ. 643, 610–622.

Baroni, G., Facchi, A., Gandolfi, C., Ortuani, B., Horeschi, D., Van Dam, J.C., 2010. Uncertainty in the determination of soil hydraulic parameters and its influence on the performance of two hydrological models of different complexity. Hydrol. Earth Syst. Sci. 14 (2), 251–270.

Barrientos, G., Herrero, A., Iroumé, A., Mardones, O., Batalla, R.J., 2020. Modelling the effects of changes in forest cover and climate on hydrology of headwater catchments in South-Central Chile. Water 12 (6), 1828. https://doi.org/10.3390/w12061828.

Bauer-Marschallinger, B., Freeman, V., Cao, S., Paulik, C., Schaufler, S., Stachl, T., Modanesi, S., Massari, C., Ciabatta, L., Brocca, L., Wagner, W., 2019. Toward global soil moisture monitoring with Sentinel-1: Harnessing assets and overcoming obstacles. IEEE Trans. Geosci. Remote Sens. 57 (1), 520–539.

Bonan, G.B., Levis, S., Sitch, S., Vertenstein, M., Oleson, K.W., 2003. A dynamic global vegetation model for use with climate models: concepts and description of simulated vegetation dynamics. Glob. Change Biol. 9 (11), 1543–1566.

Burgin, M.S., Colliander, A., Njoku, E.G., Chan, S.K., Cabot, F., Kerr, Y.H., Bindlish, R., Jackson, T.J., Entekhabi, D., Yueh, S.H., 2017. A comparative study of the SMAP passive soil moisture product with existing satellite-based soil moisture products. IEEE Trans. Geosci. Remote Sens. 55 (5), 2959–2971.

Bussi, G., Francés, F., Montoya, J.J., Julien, P.Y., 2014. Distributed sediment yield modelling: importance of initial sediment conditions. Environ. Modell. Software 58, 58–70.

Das, N. (2013). Soil Moisture Active Passive (SMAP) ancillary data report soil attributes. Jet Propulsion Lab., California Inst. of Technol., Pasadena.

Das, Narendra N., D. Entekhabi, S. Dunbar, S. Kim, S. Yueh, A. Colliander, T. J. Jackson, P. E. O'Neill, M. Cosh, T. Caldwell, J. Walker, A. Berg, T. Rowlandson, J. Martínez-Fernández, Á. González-Zamora, P. Starks, C. Holifield-Collins, J. Prueger, and E. Lopez-Baeza, November 1, 2017. Assessment Report for the L2_SM_SP Beta Release Data Products, SMAP Project, JPL D-56549, Jet Propulsion Laboratory, Pasadena, CA.

Das, N.N., Entekhabi, D., Dunbar, R.S., Chaubell, M.J., Colliander, A., Yueh, S., Jagdhuber, T., Chen, F., Crow, W., O'Neill, P.E., Walker, J.P., Berg, A., Bosch, D.D., Caldwell, T., Cosh, M.H., Collins, C.H., Lopez-Baeza, E., Thibeault, M., 2019. The SMAP and Copernicus Sentinel 1A/B microwave active-passive high resolution surface soil moisture product. Remote Sens. Environ. 233, 111380. https://doi.org/10.1016/j.rse.2019.111380.

Duan, Q., Sorooshian, S., Gupta, V., 1992. Effective and efficient global optimization for conceptual rainfall-runoff models. Water Resour. Res. 28 (4), 1015–1031.

Dembélé, M., Hrachowitz, M., Savenije, H.H.G., Mariéthoz, G., Schaefli, B., 2020a. Improving the predictive skill of a distributed hydrological model by calibration on spatial patterns with multiple satellite data sets. Water Resour. Res. 56 (1) https://doi.org/10.1029/2019WR026085.

Dembélé, M., Ceperley, N., Zwart, S.J., Salvadore, E., Mariethoz, G., Schaefli, B., 2020b. Potential of satellite and reanalysis evaporation datasets for hydrological modelling under various model calibration strategies. Adv. Water Resour. 143, 103667. https://doi.org/10.1016/j.advwatres.2020.103667.

Demirel, M.C., Mai, J., Mendiguren, G., Koch, J., Samaniego, L., Stisen, S., 2018. Combining satellite data and appropriate objective functions for improved spatial

pattern performance of a distributed hydrologic model. Hydrol. Earth Syst. Sci. 22 (2), 1299–1315.
Echeverría, C., Ruiz-Pérez, G., Puertes, C., Samaniego, L., Barrett, B., Francés, F., 2019. Assessment of Remotely Sensed Near-Surface Soil Moisture for Distributed Eco-Hydrological Model Implementation. Water 11 (12), 2613.
Escorihuela, M. J., and Quintana-Seguí, P. (2016). Comparison of remote sensing and simulated soil moisture datasets in mediterranean landscapes. Remote Sens. Environ. 180, 99–114. doi: 10.1016/j.rse.2016.02.046.
Francés F., Vélez J.I., Vélez J.J. 2007. Split-parameter structure for the automatic calibration of distributed hydrological models. Journal of Hydrology, 332 (1–2), 226-240. doi: j.jhydrol.2006.06.032.
GCOS, 2019. Global climate observing system(GCOS): essential climate variables. Retrieved 2019, 2 Dec, from. https://gcos.wmo.int/en/essential-climate-variables.
Heinsch, F. A., Reeves, M., Votava, P., Kang, S., Milesi, C., Zhao, M., et al. (2003). User's guide GPP and NPP (MOD17A2/A3) products NASA MODIS land algorithm. Version, 2, 666-684.
Hengl, T., Mendes de Jesus, J., Heuvelink, G.B.M., Ruiperez Gonzalez, M., Kilibarda, M., Blagotić, A., Shangguan, W., Wright, M.N., Geng, X., Bauer-Marschallinger, B., Guevara, M.A., Vargas, R., MacMillan, R.A., Batjes, N.H., Leenaars, J.G.B., Ribeiro, E., Wheeler, I., Mantel, S., Kempen, B., Bond-Lamberty, B., 2017. SoilGrids250m: Global gridded soil information based on machine learning. PLoS ONE 12 (2), e0169748.
Herman, J., Usher, W., 2017. SALib: An open-source Python library for Sensitivity Analysis. J. Open Source Software 2 (9), 97. https://doi.org/10.21105/joss10.21105/joss.00097.
Herman, M.R., Nejadhashemi, A.P., Abouali, M., Hernandez-Suarez, J.S., Daneshvar, F., Zhang, Z., Anderson, M.C., Sadeghi, A.M., Hain, C.R., Sharifi, A., 2018. Evaluating the role of evapotranspiration remote sensing data in improving hydrological modeling predictability. J. Hydrol. 556, 39–49.
Huscroft, J., Gleeson, T., Hartmann, J., Börker, J., 2018. Compiling and mapping global permeability of the unconsolidated and consolidated Earth: GLobal HYdrogeology MaPS 2.0 (GLHYMPS 2.0). Geophys. Res. Lett. 45 (4), 1897–1904.
Fang, L.i., Hain, C.R., Zhan, X., Anderson, M.C., 2016. An inter-comparison of soil moisture data products from satellite remote sensing and a land surface model. Int. J. Appl. Earth Obs. Geoinf. 48, 37–50.
Khaki, M., Franssen, H.J.H., Han, S.C., 2020. Multi-mission satellite remote sensing data for improving land hydrological models via data assimilation. Sci. Rep. 10 (1), 1–23.
Koch, J., Jensen, K.H., Stisen, S., 2015. Toward a true spatial model evaluation in distributed hydrological modeling: K appa statistics, F uzzy theory, and EOF-analysis benchmarked by the human perception and evaluated against a modeling case study. Water Resour. Res. 51 (2), 1225–1246.
Koch, J., Demirel, M.C., Stisen, S., 2018. The SPAtial EFficiency metric (SPAEF): multiple-component evaluation of spatial patterns for optimization of hydrological models. Geosci. Model Dev. 11 (5), 1873–1886.
Laiolo, P., Gabellani, S., Campo, L., Silvestro, F., Delogu, F., Rudari, R., Pulvirenti, L., Boni, G., Fascetti, F., Pierdicca, N., Crapolicchio, R., Hasenauer, S., Puca, S., 2016. Impact of different satellite soil moisture products on the predictions of a continuous distributed hydrological model. Int. J. Appl. Earth Obs. Geoinf. 48, 131–145.
Livneh, B., Kumar, R., Samaniego, L., 2015. Influence of soil textural properties on hydrologic fluxes in the Mississippi river basin. Hydrol. Process. 29 (21), 4638–4655.
Lopez, P.L., Sutanudjaja, E.H., Schellekens, J., Sterk, G., Bierkens, M.F.P., 2017. Calibration of a large-scale hydrological model using satellite-based soil moisture and evapotranspiration products. Hydrol. Earth Syst. Sci. 21 (6), 3125–3144. https://doi.org/10.5194/hess-21-3125-2017.
Mendiguren, G., Koch, J., Stisen, S., 2017. Spatial pattern evaluation of a calibrated national hydrological model–a remote-sensing-based diagnostic approach. Hydrol. Earth Syst. Sci. 21 (12), 5987–6005.
Manfreda, S., Fiorentino, M., Iacobellis, V., 2005. DREAM: a distributed model for runoff, evapotranspiration, and antecedent soil moisture simulation. Adv. Geosci. 2, 31–39.
Merlin, O., Escorihuela, M.J., Mayoral, M.A., Hagolle, O., Al Bitar, A., Kerr, Y., 2013. Self-calibrated evaporation-based disaggregation of SMOS soil moisture: An evaluation study at 3 km and 100 m resolution in Catalunya. Remote Sensing of Environment 130, 25–38. https://doi.org/10.1016/j.rse.2012.11.008.
Merlin, O., Rüdiger, C., Al Bitar, A., Richaume, P., Walker, J., Kerr, Y., 2012. Disaggregation of SMOS soil moisture in southeastern Australia. IEEE Transactions on Geoscience and Remote Sensing 50, 1556–1571. https://doi.org/10.1109/TGRS.2011.2175000.
Montaldo, N., Rondena, R., Albertson, J.D., Mancini, M., 2005. Parsimonious modeling of vegetation dynamics for ecohydrologic studies of water-limited ecosystems. Water Resour. Res. 41 (10) https://doi.org/10.1029/2005WR004094.
Neitsch, S.L., Arnold, J.G., Kiniry, J.R., Williams, J.R., 2011. Soil and Water Assessment Tool Theoretical Documentation Version 2009. Texas Water Resources Institute.
Ojha, N., Merlin, O., Suere, C., Escorihuela, M.J., 2021. Extending the Spatio-Temporal Applicability of DISPATCH Soil Moisture Downscaling Algorithm: A Study Case Using SMAP, MODIS and Sentinel-3 Data. Front. Environ. Sci. 9, 40.
Pablos, M., González-Haro, C., Piles, M., & BEC Team. (2020). BEC SMOS Soil Moisture Products Description (V. 1.0).
Pasquato, M., 2013. Comparison of Parsimonious Dynamic Vegetation Modeling Approaches for Semiarid Climates. Universitat Politècnica de València. PhD Thesis.
Pasquato, M., Medici, C., Friend, A. D., Francés, F., 2015. Comparing two approaches for parsimonious vegetation modelling in semiarid regions using satellite data, Ecohydrology, 8, 1024–1036, Doi: eco.1559, 2015.
Piles, M., Camps, A., Vall-llossera, M., Corbella, I., Panciera, R., Rudiger, C., Kerr, Y.H., Walker, J., 2011. Downscaling SMOS-derived soil moisture using MODIS visible/infrared data. IEEE Trans. Geosci. Remote Sens. 49 (9), 3156–3166.
Piles, M., Vall-llossera, M., Laguna, L., & Camps, A. 2012. A downscaling approach to combine SMOS multi-angular and full-polarimetric observations with MODIS VIS/IR data into high resolution soil moisture maps. Pages 1247–1250 of: IEEE International Geoscience and Remote Sensing Symposium (IGARSS) 2012.
Portal, G., Jagdhuber, T., Vall-llossera, M., Camps, A., Pablos, M., Entekhabi, D., Piles, M., 2020. Assessment of multi-scale SMOS and SMAP soil moisture products across the Iberian Peninsula. Remote Sensing 12 (3), 570.
Puertes C., Lidón A., Echeverría C, Bautista I., González-Sanchis M., del Campo A.D., Francés F. 2019. Explaining the hydrological behaviour of facultative phreatophytes using a multi-variable and multi-objective modelling approach. Journal of Hydrology, 575, 395-407. doi: j.jhydrol.2019.05.041.
Rajib, M.A., Merwade, V., Yu, Z., 2016. Multi-objective calibration of a hydrologic model using spatially distributed remotely sensed/in-situ soil moisture. J. Hydrol. 536, 192–207.
Ruiz-Pérez, G., González-Sanchis, M., Del Campo, A.D., Francés, F. 2016. Can a parsimonious model implemented with satellite data be used for modelling the vegetation dynamics and water cycle in water-controlled environments? Ecol. Modell. 324, 45–53. doi: j.ecolmodel.2016.01.002.
Ross, J., 1975. Radiative transfer in plant communities. Vegetation and the Atmosphere, 1. J. L. Monteith, Ed., Academic Press, pp. 13–55.
Ruiz-Pérez, G., Koch, J., Manfreda, S., Caylor, K., Francés, F., 2017. Calibration of a parsimonious distributed ecohydrological daily model in a data-scarce basin by exclusively using the spatio-temporal variation of NDVI. Hydrol. Earth Syst. Sci. 21 (6235–6251), 2017. https://doi.org/10.5194/hess-21-6235-2017.
Sabaghy, S., Walker, J.P., Renzullo, L.J., Akbar, R., Chan, S., Chaubell, J., Das, N., Dunbar, R.S., Entekhabi, D., Gevaert, A., Jackson, T.J., Loew, A., Merlin, O., Moghaddam, M., Peng, J., Peng, J., Piepmeier, J., Rüdiger, C., Stefan, V., Wu, X., Ye, N., Yueh, S., 2020. Comprehensive analysis of alternative downscaled soil moisture products. Remote Sens. Environ. 239, 111586. https://doi.org/10.1016/j.rse.2019.111586.
Saltelli, A., 2002. Making best use of model evaluations to compute sensitivity indices. Comput. Phys. Commun. 145 (2), 280–297.
Saltelli, A., Annoni, P., Azzini, I., Campolongo, F., Ratto, M., Tarantola, S., 2010. Variance based sensitivity analysis of model output. Design and estimator for the total sensitivity index. Comput. Phys. Commun. 181 (2), 259–270.
Silvestro, F., Gabellani, S., Rudari, R., Delogu, F., Laiolo, P., Boni, G., 2015. Uncertainty reduction and parameter estimation of a distributed hydrological model with ground and remote-sensing data. Hydrol. Earth Syst. Sci. 19 (4), 1727–1751.
Sitch, S., Smith, B., Prentice, I.C., Arneth, A., Bondeau, A., Cramer, W., Kaplan, J.O., Levis, S., Lucht, W., Sykes, M.T., Thonicke, K., Venevsky, S., 2003. Evaluation of ecosystem dynamics, plant geography and terrestrial carbon cycling in the LPJ dynamic global vegetation model. Global Change Biology 9, 161–185. https://doi.org/10.1046/j.1365-2486.2003.00569.x.
Sobol′, I.M., 2001. Global sensitivity indices for nonlinear mathematical models and their Monte Carlo estimates. Math. Comput. Simul 55 (1-3), 271–280.
Song, X., Zhang, J., Zhan, C., Xuan, Y., Ye, M., Xu, C., 2015. Global sensitivity analysis in hydrological modeling: review of concepts, methods, theoretical framework, and applications. J. Hydrol. 523, 739–757.
Tang, Y., Reed, P., Wagener, T., Werkhoven, K.V., 2007. Comparing sensitivity analysis methods to advance lumped watershed model identification and evaluation. Hydrol. Earth Syst. Sci. 11 (2), 793–817.
Tóth, B., Weynants, M., Pásztor, L., Hengl, T., 2017. 3D soil hydraulic database of Europe at 250 m resolution. Hydrol. Process. 31 (14), 2662–2666.
Vrugt, J.A., Gupta, H.V., Bastidas, L.A., Bouten, W., Sorooshian, S., 2003a. Effective and efficient algorithm for multiobjective optimization of hydrologic models. Water Resour. Res. 39 (8) https://doi.org/10.1029/2002WR001746.
Vrugt, J.A., Gupta, H.V., Bouten, W., Sorooshian, S., 2003b. A Shuffled Complex Evolution Metropolis algorithm for optimization and uncertainty assessment of hydrologic model parameters. Water Resour. Res. 39 (8) https://doi.org/10.1029/2002WR001642.
Wambura, F.J., Dietrich, O., Lischeid, G., 2018. Improving a distributed hydrological model using evapotranspiration-related boundary conditions as additional constraints in a data-scarce river basin. Hydrol. Process. 32 (6), 759–775.
Wanders, N., Bierkens, M.F.P., de Jong, S.M., de Roo, A., Karssenberg, D., 2014. The benefits of using remotely sensed soil moisture in parameter identification of large-scale hydrological models. Water Resour. Res. 50 (8), 6874–6891.
Wang, G., Zhang, X., Yinglan, A., Duan, L., Xue, B., Liu, T., 2021. A spatio-temporal cross comparison framework for the accuracies of remotely sensed soil moisture products in a climate-sensitive grassland region. J. Hydrol. 597, 126089. https://doi.org/10.1016/j.jhydrol.2021.126089.
Wagner, W., 1998. Soil moisture retrieval from ERS scatterometer data. European Commission, Joint Research Centre, Space Applications Institute.
Williams, C.A., Albertson, J.D., 2005. Contrasting short-and long-timescale effects of vegetation dynamics on water and carbon fluxes in water-limited ecosystems. Water Resour. Res. 41 (6) https://doi.org/10.1029/2004WR003750.
Zhang, C., Chu, J., Fu, G., 2013. Sobol′'s sensitivity analysis for a distributed hydrological model of Yichun River Basin, China. J. Hydrol. 480, 58–68.
Zhang, L., Hu, Z., Fan, J., Zhou, D., Tang, F., 2014. A meta-analysis of the canopy light extinction coefficient in terrestrial ecosystems. Frontiers of earth science 8 (4), 599–609.
Zink, M., Mai, J., Cuntz, M., Samaniego, L., 2018. Conditioning a hydrologic model using patterns of remotely sensed land surface temperature. Water Resour. Res. 54 (4), 2976–2998.
Zitzler, E., Thiele, L., 1999. Multiobjective evolutionary algorithms: a comparative case study and the strength Pareto approach. IEEE Trans. Evol. Comput. 3 (4), 257–271.